Neurobiology of Disease 180 (2023) 106093

Contents lists available at ScienceDirect

Neurobiology of Disease

journal homepage: www.elsevier.com/locate/ynbdi

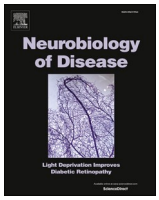

Myelin basic protein recovery during PKU mice lifespan and the potential role of microRNAs on its regulation

Alessandro Bregalda [a,*], Claudia Carducci [b], Maria Teresa Viscomi [c,d], Francesca Pierigè [a], Sara Biagiotti [a], Michele Menotta [a], Federica Biancucci [a], Tiziana Pascucci [e,f], Vincenzo Leuzzi [g], Mauro Magnani [a,h], Luigia Rossi [a,h]

[a] Department of Biomolecular Sciences, University of Urbino "Carlo Bo", via Saffi 2, 61029 Urbino, PU, Italy
[b] Department of Experimental Medicine, Sapienza University, viale del Policlinico 155, 00161 Rome, Italy
[c] Department of Life Sciences and Public Health, Sect. Histology and Embryology, Catholic University of the Sacred Heart, Largo F. Vito 1, 00168 Rome, Italy
[d] Fondazione Policlinico Universitario "Agostino Gemelli", IRCCS, 00168 Rome, Italy
[e] Fondazione Santa Lucia IRCCS, via Ardeatina 306, 00142 Rome, Italy
[f] Department of Psychology and Centro "Daniel Bovet", Sapienza University, via dei Marsi 78, 00185 Rome, Italy.
[g] Department of Human Neuroscience, Sapienza University, via dei Sabelli 108, 00185 Rome, Italy
[h] EryDel SpA, via Antonio Meucci 3, 20091 Bresso, Milan, Italy.

ARTICLE INFO

Keywords:
Myelin basic protein
Phenylketonuria
MicroRNA
Microarray
Mouse maturation
Cerebral plasticity

ABSTRACT

Untreated phenylketonuria (PKU) patients and PKU animal models show hypomyelination in the central nervous system and white matter damages, which are accompanied by myelin basic protein (MBP) impairment. Despite many assumptions, the primary explanation of the mentioned cerebral outcomes remains elusive. In this study, MBP protein and mRNA expression on brains of wild type (WT) and phenylketonuric (ENU2) mice were analyzed throughout mice lifespan (14-60-180-270-360-540 post-natal days, PND). The results confirmed the low MBP expression at first PND times, while revealed an unprecedented progressive MBP protein expression recovery in aged ENU2 mice. Unexpectedly, unaltered MBP mRNA expression between WT and ENU2 was always observed. Additionally, for the same time intervals, a significant decrease of the phenylalanine concentration in the peripheral blood and brain of ENU2 mice was detected, to date, for the first time. In this scenario, a translational hindrance of MBP during initial and late cerebral development in ENU2 mice was hypothesized, leading to the execution of a microRNA microarray analysis on 60 PND brains, which was followed by a proteomic assay on 60 and 360 PND brains in order to validate *in silico* miRNA-target predictions. Taken together, miR-218-1-3p, miR-1231-3p and miR-217-5p were considered as the most impactful microRNAs, since a downregulation of their potential targets (MAG, CNTNAP2 and ANLN, respectively) can indirectly lead to a low MBP protein expression. These miRNAs, in addition, follow an opposite expression trend compared to MBP during adulthood, and their target proteins revealed a complete normalization in aged ENU2 mice. In conclusion, these results provide a new perspective on the PKU pathophysiology understanding and on a possible treatment, emphasizing the potential modulating role of differentially expressed microRNAs in MBP expression on PKU brains during PKU mouse lifespan.

1. Introduction

Phenylketonuria (PKU; OMIM 261600) is a rare autosomal inherited disorder characterized by a defect in the phenylalanine hydroxylase (PAH, phenylalanine 4-monooxygenase, EC 1.14.16.1) functionality. This enzyme is actively expressed in the liver, and it is fundamental in the metabolism of the essential amino acid Phenylalanine (L-Phe). The reaction consists of a hydroxylation of L-Phe into Tyrosine (L-Tyr) in the presence of tetrahydrobiopterin as cofactor. Mutations affecting PAH gene result in an altered enzyme, leading to L-Phe accumulation (hyperphenylalaninemia, HPA) in the peripheral blood and in the brain, besides to a reduced concentration of L-Tyr and its derivatives (van Spronsen et al., 2021). L-Phe excess causes severe neurodevelopmental impairment, leading to permanent neurological damages, intellectual

* Corresponding author.
E-mail address: alessandro.bregalda@uniurb.it (A. Bregalda).

https://doi.org/10.1016/j.nbd.2023.106093
Received 1 February 2023; Received in revised form 10 March 2023; Accepted 17 March 2023
Available online 21 March 2023

disability, seizures, and behavioral problems.

Among the neurological defects reported in untreated PKU patients and animal models (i.e. ENU2 mice), white matter alterations in the central nervous system (CNS) are a common denominator (Anderson and Leuzzi, 2010; Klippel et al., 2021). One of the main aspects that could have an impact on the neuropathological symptoms is the observed hypomyelination or demyelination of the CNS axons, the cause of which remains elusive (Schoemans et al., 2010; González et al., 2018). Indeed, many assumptions have been made, ranging from abnormal epigenetic modifications (Dobrowolski et al., 2015, 2016) to cytotoxic damage caused by oxidative stress (Bortoluzzi et al., 2021; Dobrowolski et al., 2022). Other hypotheses are an impaired cholesterol metabolism (Shefer et al., 2000; Guerra et al., 2020) and/or defects in calcium homeostasis (Yu et al., 2007; Schuck et al., 2015), which add to abnormal brain proteins synthesis and composition, especially at the myelin sheath level (Park et al., 2009; Li et al., 2010; Hong et al., 2021). Preclinical studies show that myelin basic protein (MBP, ENSG00000197971), a fundamental structural protein of the myelin sheath, is downregulated in the presence of high levels of L-Phe in the peripheral blood, resulting in defective myelination (Baba et al., 1987; Dyer et al., 1996; Pascucci et al., 2018), which may be prevented (Rossi et al., 2014; Pascucci et al., 2018) or reversed (Burri et al., 1990) by lowering blood L-Phe levels. Predominantly expressed by oligodendrocytes (OLs) in the corpus callosum and in the cerebral cortex, MBP is the second most abundant protein in the myelin compartment, and it is crucial for the correct assembling of the myelin leaflets. In fact, thanks to its positive charge due to its basic character, the protein is pivotal in the adhesion of the cytosolic surfaces of multilayered compact myelin and its impaired functionality can result in shivering symptoms, severe hypomyelination, seizures and early death (Campagnoni and Macklin, 1988; Campagnoni et al., 1993; Boggs, 2006). MBP translation occurs in the myelin compartment, thanks to the MBP mRNA transport from nucleus to the cellular membrane inside RNA transport granules that move along microtubules (Lyons et al., 2009; Müller et al., 2013; Herbert et al., 2017). MBP expression is also regulated by cis- and trans-acting factors which contribute to its translation both locally and temporally (Laursen et al., 2011; Bauer et al., 2012; Müller et al., 2013; Torvund-Jensen et al., 2014). In fact, MBP mRNA can be already detected in immature oligodendrocytes which do not yet synthesize MBP protein, therefore MBP translation could be repressed in immature OLs until a minimum degree of differentiation is achieved. In addition, the protein itself interacts with plenty of proteins such as proteolipid protein 1 (PLP1), calmodulin (CAM), actin (ACTB), L1 cell adhesion molecule (L1CAM), clathrin heavy chain (CLTC), 2′,3′-cyclic nucleotide 3′ phosphodiesterase (CNP) and contactin (CNTN), thus demonstrating its key role in the neural network (Smirnova et al., 2021).

Among the possible elucidations about the negative neurological outcomes observed in PKU patients, abnormal epigenetic modifications play an important role. In fact, aberrant DNA methylation has been observed in postmortem brains of PKU patients and an extensive epigenome repatterning has been detected in the CNS of ENU2 mice (Dobrowolski et al., 2015, 2016). These epigenetic modifications may lead to an abnormal expression of important proteins involved in many neurological processes, such as axon guidance, synaptic transmission, and dendritic spines development (Huttenlocher, 2000), contributing to explain the abnormal synaptogenesis and the altered dendritic development found in PKU patients and in the animal models of disease (Huttenlocher, 2000; Baumann and Pham-Dinh, 2001; Andolina et al., 2011). Interestingly, L-Phe restricted diet in ENU2 mice displayed an attenuated pattern of aberrant DNA methylation, highlighting the fact that high L-Phe toxic exposure can modify the brain epigenome leading, in turn, to hyper- or hypomethylated gene coding regions (Dobrowolski et al., 2016). Among the latter, differential DNA methylation has been observed in genomic loci enriched in microRNAs (miRNAs), which are able to inhibit the translation or to degrade target mRNAs via base pairing to complementary sites in the target mRNA 3′-UTR (Bartel, 2004). Therefore, miRNAs dysregulation in PKU mice and patients may have secondary effects upon the expression of targeted proteins (Dobrowolski et al., 2016). It should be noted that several miRNAs are involved in OLs development and myelination, thus playing a fundamental role in the outcomes of several demyelinating diseases such as multiple sclerosis (Gandhi, 2015; Galloway and Moore, 2016).

In the current study, MBP expression was examined in the untreated ENU2 animal model from 14 to 540 PND. Moreover, the occurrence of up- or downregulated miRNAs that could interfere with MBP production during this lifespan was investigated. Briefly, it has been shown for the first time that while MBP synthesis was depressed during ENU2 brain development, a normal level of MBP was restored in a more mature brain. Moreover, a complete normalization of multiple cerebral proteins during adulthood, linking the miRNAs' potential downregulating effects to their respective targets, has been found. Taken together, this preclinical longitudinal analysis over a prolonged period is aimed to figure out which are the main causes that could lead to hypomyelination and MBP downregulation in the ENU2 mouse brain, learning more about the potential pathophysiological role of miRNAs on PKU cerebral outcomes and, consequently, paving the way to alternative PKU treatments (i.e. miRNAs gene therapy and/or epigenetic reprogramming (Bale, 2015; Fu et al., 2019; Grisch-Chan et al., 2019; Tao et al., 2020)).

2. Materials and methods

2.1. Animals

BTBR mice have been raised in the animal shelter of the Biochemistry and Biotechnology section of the Department of Biomolecular Sciences of the University of Urbino Carlo Bo. $PAH^{Enu2(-/-)}$ (ENU2) and $PAH^{Enu2(+/+)}$ (wild type; WT) male mice used in this study were obtained from mating between heterozygous animals belonging to the BTBR strain. The animals were housed in standard cages, from 3 to 6 mice per cage, with a light-dark cycle of 12 h and under controlled conditions of temperature (22 ± 1 °C), humidity (60%) and air change (every 12 h). Genetic characterization was performed as described (McDonald and Charlton, 1997). All mice were fed with a Teklad global 18% protein rodent diet (Teklad, Harlan Laboratories Inc., Madison, WI) and water ad libitum. All the experiments were conducted in accordance with the European legislation (2010/63/EU), with the Italian national legislation (DL26/2014) which governs the use of animals for research and with the guidelines of the National Institute of Health on the use and the care of laboratory animals (Authorization n° 486/2017-PR).

2.2. Western blotting

WT and ENU2 brains of different PND (see Table 1) were collected and snap frozen immediately in liquid nitrogen after washing in phosphate buffered saline (PBS). 30 mg of brain tissues were then homogenized in RIPA buffer (Milli-Q Water, 0.05 M Tris Hydrochloride pH 7.4, 0.001 M Potassium Chloride, 0.0015 M Magnesium Chloride, 0.001 M EDTA, 0.001 M Dithiothreitol, 0.005 M Sodium Fluoride, 0.001 M Sodium Metavanadate, 0.1% SDS) with 10% Sodium Deoxycholate (Na-DOC), 1% Triton X − 100 and 1× cOmplete™ Protease Inhibitor

Table 1
Mice brains numerosity utilized in this work.

Mice post-natal days	N samples per genotype	
	WT	ENU2
14 PND	6	4
60 PND	5	9
180 PND	5	5
270 PND	5	5
360 PND	6	6
540 PND	4	6

Cocktail (Roche) for the subsequent Western Blotting (WB) procedure. Samples were kept on ice for 20 min and then sonicated 30s at 50 W with pulse mode.

After centrifugation (15 min at 4 °C, 12200 *g*), supernatants were collected, and proteins were quantified using Bradford assay. 10 μg of total proteins from each sample were loaded onto 8–12% polyacrylamide gels for SDS-PAGE. After 1 h running (40 mA), gels were placed in sandwich cassettes with nitrocellulose membranes and submitted to the blotting transfer procedure for 70 min at 100 V. Electrophoretic transfer output was assessed with Ponceau S staining (0.1% Ponceau S (*w/v*) in 5% (*v*/v) acetic acid) at the ChemiDoc Imaging System (Bio-Rad). Membranes were then blocked with with Tris-buffered saline (TBS)/5% non-fat dry milk for 1 h and incubated ON with the proper primary antibodies diluted in Tween 0.1%-Tris-buffered saline (TTBS)/5% non-fat dry milk (Table 2A). The next day, membranes were washed 3 times (10 min each) with TTBS and then incubated 1 h at room temperature with the appropriate secondary antibodies (Table 2B). After that, membranes were washed again 3 times with TTBS (10 min each) and then exposed to the ChemiDoc Imaging System using the enhanced chemiluminescence (ECL) procedure after 2 min incubation with a mixture of H_2O_2 and luminol substrate (WesternBright™ ECL, K-12045-D20; Advansta). Protein bands intensities were acquired through densitometric analysis and the immunoblots were quantified using Image Lab software (Bio-Rad). Mean ratios between MBP, Myelin PLP1, MAG, ANLN and CNTNAP2 bands intensity were reported as percentage of control values, with β-Actin as loading control.

2.3. Immunofluorescence and densitometric analysis of fluorescence images

WT and ENU2 brain hemispheres of young and adult WT and ENU2 mice were collected and soaked in paraformaldehyde 4% with overnight incubation for tissue fixation. After 24 h, brains were put in sucrose 30% and left at 4 °C until precipitation. Brain sections were then incubated overnight with a cocktail of primary antibodies, including rat anti-MBP (Abcam #ab7349), and rabbit anti-PLP1 (Abcam #28846) in a solution of PBS and 0.3% Triton X − 100, followed by a cocktail of secondary antibodies (1:200, Invitrogen), including Alexa Fluor 555 conjugated donkey anti-rat and Alexa Fluor 488 conjugated donkey anti-rabbit. Sections were examined under a confocal laser scanning microscope (Leica SP5). Densitometric analysis of MBP and PLP1 was performed on 5 brain sections per mice (at the level of the striatum). Specifically, MBP- and PLP1-associated signals were quantified by manually outlining the area of interest. Mean signal intensity (F) of the marker of interest was performed on two squared frames (35 μm per side) on 5 sections sampled to cover the rostro-caudal extent of the areas of interest (striatum and corpus callosum) entirely ($n = 10$ samples per mouse). The F/A ratio defines mean fluorescence of individual samples (F) normalized to total cellular surface (A).

Table 2
List of the primary (A) and secondary (B) antibodies utilized in Western Blot analyses.

Description	Catalogue Number	Host	Dilution in TTBS/5% non-fat dry milk	Supplier
(A)				
Anti-Myelin Basic Protein (MBP)	MAB386	Rat	1:1000	Merck-Millipore
Anti-Myelin Proteolipid Protein (PLP1)	#85971	Rabbit	1:500	Cell Signaling Technology
Anti-Myelin-Associate Glycoprotein (MAG)	#346200	Rabbit	1:1000	Thermo Fisher Scientific
Anti-Anillin (ANLN)	PA5114851	Rabbit	1:500	Thermo Fisher Scientific
Anti-Contactin Associated Protein 2 (CNTNAP2)	PA528969	Rabbit	1:5000	Thermo Fisher Scientific
Anti-β-Actin (ACTB)	8H10D10	Mouse	1:1000	Cell Signaling Technology
(B)				
Donkey anti-rat-IgG-HRP	AP189P	Donkey	1:2000	Merck Millipore
Goat anti-rabbit-IgG-HRP	sc-2004	Goat	1:2000	Santa Cruz Biotechnology
Goat anti-mouse-IgG (H + L)-HRP	170–6516	Goat	1:2000	Bio-Rad

2.4. RT-qPCR

WT and ENU2 brains of different PND (see Table 1, *no 540 PND*) were collected and snap frozen immediately in liquid nitrogen after washing in PBS. After homogenization, whole brain lysates (30 mg) were treated for RNA extraction using the RNeasy Plus Mini Kit (QIAGEN) following the manufacturer's instructions. RNA samples were quantified using Nanodrop® ND − 100 Spectrophotometer (Thermo Fisher Scientific), keeping A260/A280 and A260/A230 ratios between 1.8 and 2.2 as critical values for evaluating RNA purity and possible contaminants. Subsequently, retrotranscription procedure was performed taking 500 ng from each RNA sample using the PrimeScript™ RT Master Mix (Takara Bio Inc.), following the manufacturer's instructions. cDNA samples were then diluted in DNAse-free H_2O to have 10 ng/μl to be used in the qPCR for the MBP mRNA quantification. For each cDNA sample from WT and ENU2 brains of different ages, the reaction mix was settled using TaqMan probes specific for MBP (Mm01266402_m1, Thermo Fisher Scientific) and HPRT (Mm03024075_m1, Thermo Fisher Scientific). 10 μl of mix with cDNA from each sample were loaded in a reaction plate (final volume: 20 μl) and then put in the 7500 Applied Biosystem machine for cDNA amplification. Results expressed in $2^{-\Delta\Delta Ct}$ were used for the subsequent relative quantification of MBP mRNA expression levels, using HPRT as housekeeping gene.

2.5. L-PHE and L-TYR evaluation in dried blood spot (DBS)

Mouse whole blood was collected on Whatman TM 903, dried under ambient conditions, and stored at −80 °C in plastic bags. A 3-mm diameter dot was punched from the DBS into a single well of 96-well micro plate. The analysis of L-Phe and L-Tyr in the DBS was performed using a previously published method (Chace et al., 1993) with some modifications (Rossi et al., 2014).

2.6. Brain L-PHE and L-TYR evaluation

For brain L-Phe and L-Tyr quantification, frozen brain samples were weighted and homogenized in 0.1 N $HClO_4$ (Carlo Erba) containing Na-metabisulphite (Carlo Erba) and 1 mM EDTA (Carlo Erba), in order to have a ratio of 1:100 ml/mg. Homogenates were then centrifuged at 10000 *g* for 20 min at 4 °C. Supernatants were collected and subsequently transferred to the 1200 series HPLC system (Agilent Technologies, CA, United States). The analysis was performed using the method published by Carducci et al. (Carducci et al., 1996) with some modifications. Chromatographic separation was accomplished with Hypersil AA ODS 2.1 × 200 mm (5 μm) column coupled with an ODS Hypersil ODS guard column 20 × 4 mm I.D. (Agilent Technologies, CA, United States). Mobile phase A was 20 mM sodium acetate buffer (pH 7.2) containing triethylamine 0.044% (*v*/v), while mobile phase B was a solution of 100 mM sodium acetate buffer (pH 7.2), acetonitrile and methanol (1:2:2, v/v/v) (Sigma-Aldrich, MO, United States). A gradient elution was applied (Supplementary Material Table 1). The flow rate

was 0.45 mL/min and the column temperature was 38 °C.

2.7. miRNA microarray and miRNA RT-qPCR

Selected WT and ENU2 brain lysates of 60 PND (WT, $n = 4$; ENU2, n = 4) were prepared in QIAzol reagent and total RNA from each sample was extracted with miRNeasy Mini Kit (QIAGEN) according to the manufacturer's instructions. RNA samples were quantified using Nanodrop® ND − 100 Spectrophotometer (Thermo Fisher Scientific), keeping A260/A280 and A260/A230 ratios between 1.8 and 2.2 as critical values for evaluating RNA purity and possible contaminants. Total RNA was further analyzed by denaturing gradient gel electrophoresis (agarose 1.3%, formaldehyde 2.2 M, MOPS 1×), with the purpose of checking RNA integrity and the possible presence of genomic DNA. miRNAs' expression profile in WT and ENU2 was performed according to the manufacturer's protocols (Affymetrix, Santa Clara, CA, United States) by Cogentech Affymetrix microarray unit (Campus IFOM-IEO, Milan, Italy) using *Mus Musculus* Affymetrix GeneChip miRNA 4.0 (Affymetrix). The different gene expression patterns were analyzed by using Partek Genomics Suite updated to version 7019 (Partek®). PCA (Principal Component Analysis) was carried out to highlight differentially expressed miRNAs and the normalized background-corrected data were transformed to the log2 scale. Unpaired *t*-test was performed to determine which miRNAs were modulated at a significance level ($P < 0.05$) and statistically significant miRNAs were selected for final consideration when their expression was at least 1.2-fold different between ENU2 and WT samples.

For microarray validation of 60 PND miRNAs and and miRNAs evaluation during mouse growth, total RNA from WT and ENU2 brain lysates of different ages (14-60-180-270-360 PND, $n = 4$/condition) was extracted as displayed previously. miRNA RT-qPCR from total RNA were performed using the TaqMan® MicroRNA Reverse Transcription Kit together with the TaqMan® MicroRNA Assays (both from Thermo Fisher Scientific) specific for the miRNA of interest. Retrotranscription and qPCR were carried out following manufacturer's instructions. Briefly, 10 ng of total RNA were retrotranscribed and 1.34 μl of the RT reaction product were placed into each tube with the qPCR reaction mix. The reaction mix was then loaded in the 7500 Applied Biosystem machine for cDNA amplification. Results expressed in $2^{-\Delta\Delta Ct}$ were used for the subsequent relative quantification of the selected miRNAs (mmu-miR-217-5p, MIMAT0000679_st; mmu-miR-671-3p, MIMAT0004821_st; mmu-miR-448-5p, MIMAT0017176_st; mmu-miR-1231-3p, MIMAT0022358_st; mmu-miR-218-1-3p, MIMAT0004665_st; mmu-miR-715, miRBase Version v22.1; snoRNA202, AF357327), using snoRNA202 as endogenous control.

2.8. Proteomic analyses on WT and ENU2 brains

20 μg of each selected WT and ENU2 brain lysates of 60 and 360 PND (WT, n = 4; ENU2, n = 4 per age) were processed by EasyPep MS Sample Kit (Thermo Scientific Pierce) by the TMT (Tandem Mass Tag) labeling option (16plex TMTpro, Thermo Fisher Scientific) and finally mixed in equimolar ratio. The sample was fractionated by Pierce High pH Reversed-Phase Peptide Fractionation Kit. Subsequently, drying fractions were dissolved in water 0.1% formic acid and 2 μg were injected in an UltiMate 3000 RSLC nano system coupled to the Exploris 240 mass spectrometer. Briefly, peptides were desalted online by Acclaim PepMap C18 Reversed Phase HPLC Column (5 μm, 0.3 mm × 5 mm Thermo Fisher Scientific), and then resolved by Easy-Spray Pepmap RSLC C18 (2 μm, 50 cm × 75 μm) at a flow rate of 300 nl/min with a gradient of phase B (80% acetonitrile/0.1% formic acid, solvent A was 0.1% formic acid in water) from 2% to 40% in 220 min. Then (B) was changed up 99% in 12 min, kept for 7 min, and then the column was re-equilibrated for 10 min. Data were acquired in a positive mode and data-dependent manner. For MS1 *m/z* range was set to 350–1500 at 120,000 resolution (at m/z 200), ACG target 3e6, and auto maximum injection time. MS2 was adopted when ions intensity was above 5e3, with m/z range in auto mode, normalized HCD energy 35%, ACG target 7.5e4, and maximum injection time 40 ms. The resolution was set to 15,000 at m/z 200 and the internal calibrant was employed in run start mode. Fractions were analyzed in quadruplicates and raw data were employed in Proteome Discoverer software v2.5 adopting the TMT signal quantification strategy. Master proteins were considered differentially expressed with a fold change 1.5 and FDR < 0.1 (False Discovery Rate).

2.9. Bioinformatic analyses

2.9.1. miRNAs' targets prediction networks

Predicted target genes of the mature upregulated (fc > 1.2) and downregulated (fc > 2.5) miRNAs in ENU2 were evaluated using three online databases: miRDB (Chen and Wang, 2020) (>70 target score cutoff), TargetScanMouse 8.0 (Agarwal et al., 2015) (<-30 total context++ score cutoff) and DIANA TOOLS-microT-CDS (Paraskevopoulou et al., 2013) (>0.7 miTG score cutoff). Only the target genes which were common in the prediction of all the above algorithms were used in the building of the miRNAs-predicted targets networks through Cytoscape v3.9.1 software (Shannon et al., 2003) and in the preliminary targets' functional evaluation through gene set enrichment analysis (GSEA) with ShinyGO v0.76 (Ge et al., 2020) (http://bioinformatics.sdstate.edu/go/), using the Benjamini-Hochberg FDR adjusted *p*-value ($p < 0.05$).

2.9.2. Protein-protein interaction and GSEA on ENU2 cerebral proteins

Protein-protein interaction (PPI) networks for the up- and downregulated proteins in ENU2 brains of 60 PND detected from the proteomic analysis were constructed using the Cytoscape v3.9.1 built-in stringAPP, with minimum required interaction score set to medium confidence (>0.4) (Shannon et al., 2003; Szklarczyk et al., 2019). The resulting network was then analyzed through the Cytoscape plug-in MCODE in order to detect significant clusters and subnetworks among the principal one (Node Density Cutoff: 0.1; Node Score Cutoff: 0.2; K-Core: 2; Max Depth: 100) (Bader and Hogue, 2003). Gene set enrichment analyses over up- and downregulated proteins in ENU2 brains were performed through ShinyGO v0.76 (Ge et al., 2020) (http://bioinformatics.sdstate.edu/go/) using the Benjamini-Hochberg FDR adjusted p-value ($p < 0.05$).

2.10. Statistical analyses

Statistical analyses were performed with GraphPad Prism 8.0.1 (GraphPad Software, La Jolla, CA, USA) using two-way ANOVA in case of more than two groups to be measured or two-tailed *t*-test when each measure had only two groups. *P*-value threshold for significance was set to $p < 0.05$. The data are shown as Mean ± SEM.

3. Results

3.1. MBP levels increase during ENU2 mice lifespan, while MBP mRNA remains unaltered

In order to evaluate the possible MBP downregulation during the lifetime of PKU mice, WBs from WT and ENU2 mice brain lysates of various ages (14-60-180-270-360-540 PND) were performed. As reported in Fig. 1A-B, MBP levels are significantly lower in ENU2 compared to WT mice at 14 and 60 PND (−64.5% and − 70%, with $p = 0.043$ and $p = 0.022$, respectively). However, at 180, 270, 360 and 540 PND, a recovery of the MBP protein levels in middle-aged ENU2 mice was observed (−50.9%, −20.4%, −14.7%, −9.1% respectively), almost returning to the protein levels observed in healthy WT mice. The reported multiple bands confirmed the four main MBP isoforms in the mouse (Boggs, 2006) and allowed MBP quantification through mean of the sum of their intensities. Together, myelin PLP1 (the most abundant

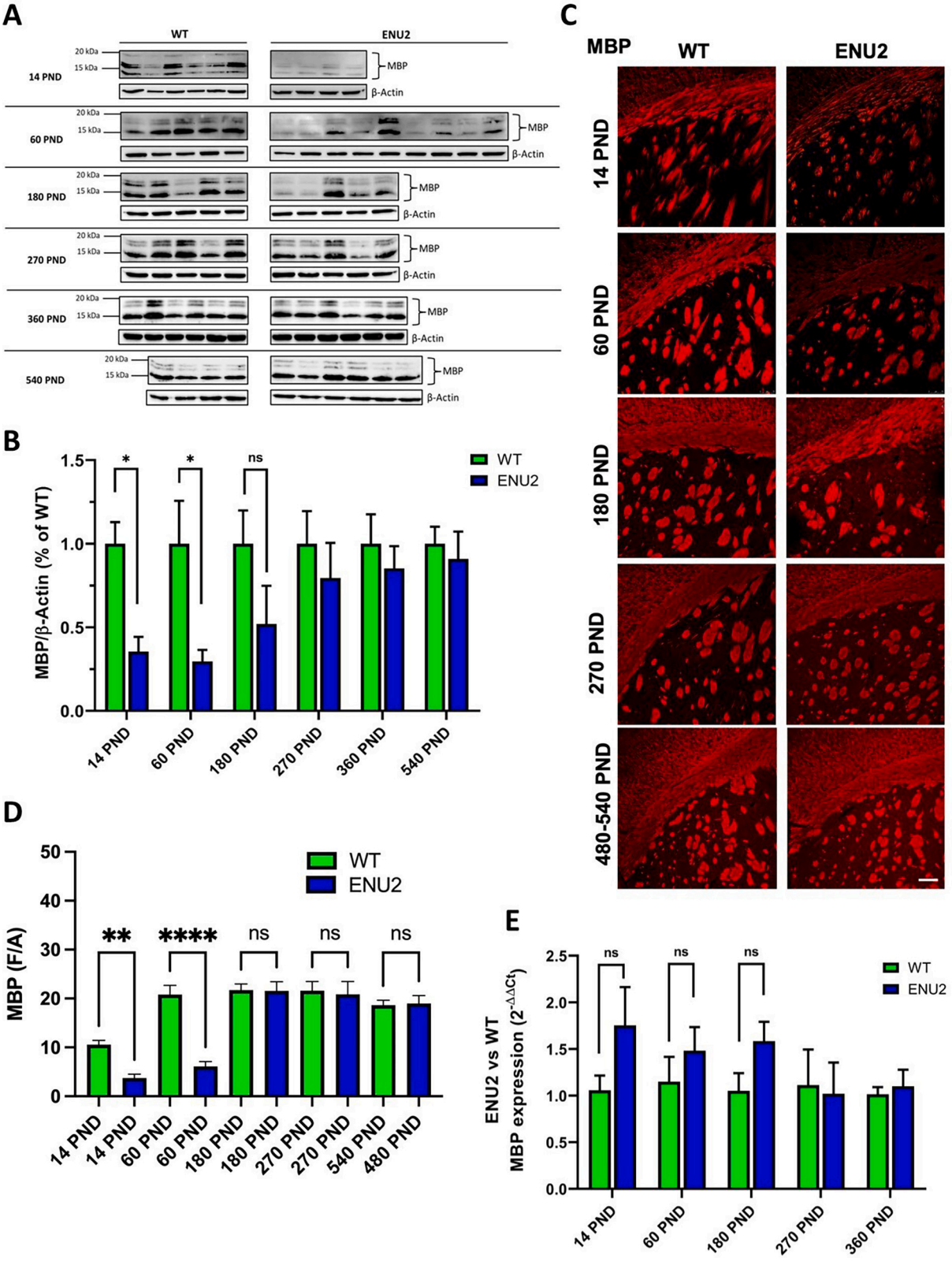

(caption on next page)

Fig. 1. Representative immunoblots (A) and densitometric analysis (B) of MBP protein showing the expression levels in WT and ENU2 brains. MBP protein levels reached almost normal expression compared to WT in middle-aged and aged ENU2 mice. Each lane corresponds to a different animal. Data are expressed as Mean ± SEM (14 PND, WT $n = 6$, ENU2 $n = 4$; 60 PND, WT $n = 5$, ENU2 $n = 9$; 180 PND, WT n = 5, ENU2 n = 5; 270 PND, WT n = 5, ENU2 n = 5; 360 PND, WT n = 6, ENU2 n = 6). All the reported values in the graph are densitometric values obtained calculating the mean of the sum between the relative intensities of each band using Image Lab software. Bands are placed at known molecular weights (14.5–21 kDa). Two-way ANOVA followed by Bonferroni's multiple comparisons test, *$p < 0.05$. (C) Confocal images and relative densitometric results (D) of the expression levels of MBP in the two experimental groups of mice at different ages. Expression levels of MBP at 60 PND in ENU2 brain are significantly lower compared to 60 PND WT mice and its expression in adult mice shows no statistical differences between conditions. The F/A ratio defines mean fluorescence of individual samples (F) normalized to total cellular surface (A). Two-way ANOVA followed by Bonferroni's multiple comparison test, *p < 0.05; **$p < 0.01$; ***$p < 0.001$; ****$p < 0.0001$. (E) RT-qPCR of relative MBP mRNA expression in WT and ENU2 brains. No differences were detected in both condition during mice lifespan. Data are expressed as Mean ± SEM (14 PND, WT n = 6, ENU2 n = 4; 60 PND, WT n = 5, ENU2 n = 9; 180 PND, WT $n = 5$, ENU2 $n = 5$; 270 PND, WT n = 5, ENU2 n = 5; 360 PND, WT n = 6, ENU2 n = 6). HPRT has been used as endogenous control. Two-way ANOVA followed by Bonferroni's multiple comparisons test, *$p < 0.05$.

myelin protein (Baron et al., 2015; Jahn et al., 2020)) immunoblots and densitometric analysis revealed a slight PLP1 protein reduction in ENU2 brain lysates of 14–60 PND (−51%, −19.8%, respectively), although the obtained results were not statistically significant (Supplementary Material Fig. S1A). In order to confirm and further validate WBs densitometric results, a confocal analysis of the immunofluorescence (IF) stained sections −5 brain sections per mice at the level of the striatum-was performed. Provided results (Fig. 1C-D) confirmed data already obtained through WBs, with a MBP staining that is significantly lower in ENU2 mice at 14–60 PND and an almost complete recovery of the MBP staining during adulthood. On the other hand, PLP1 resulted to be unaltered in both conditions on the evaluated time points (Supplementary Material Fig. S1B), with a slight decrease (even not significant) observable in ENU2 mice at 60-180-540 PND. Taken together, these data could indicate a specific hindrance only over MBP expression, with no relevance over PLP1 expression.

We then hypothesized that low protein levels could correspond to a reduced amount of the MBP mRNA expression levels. To do so, RT-qPCR

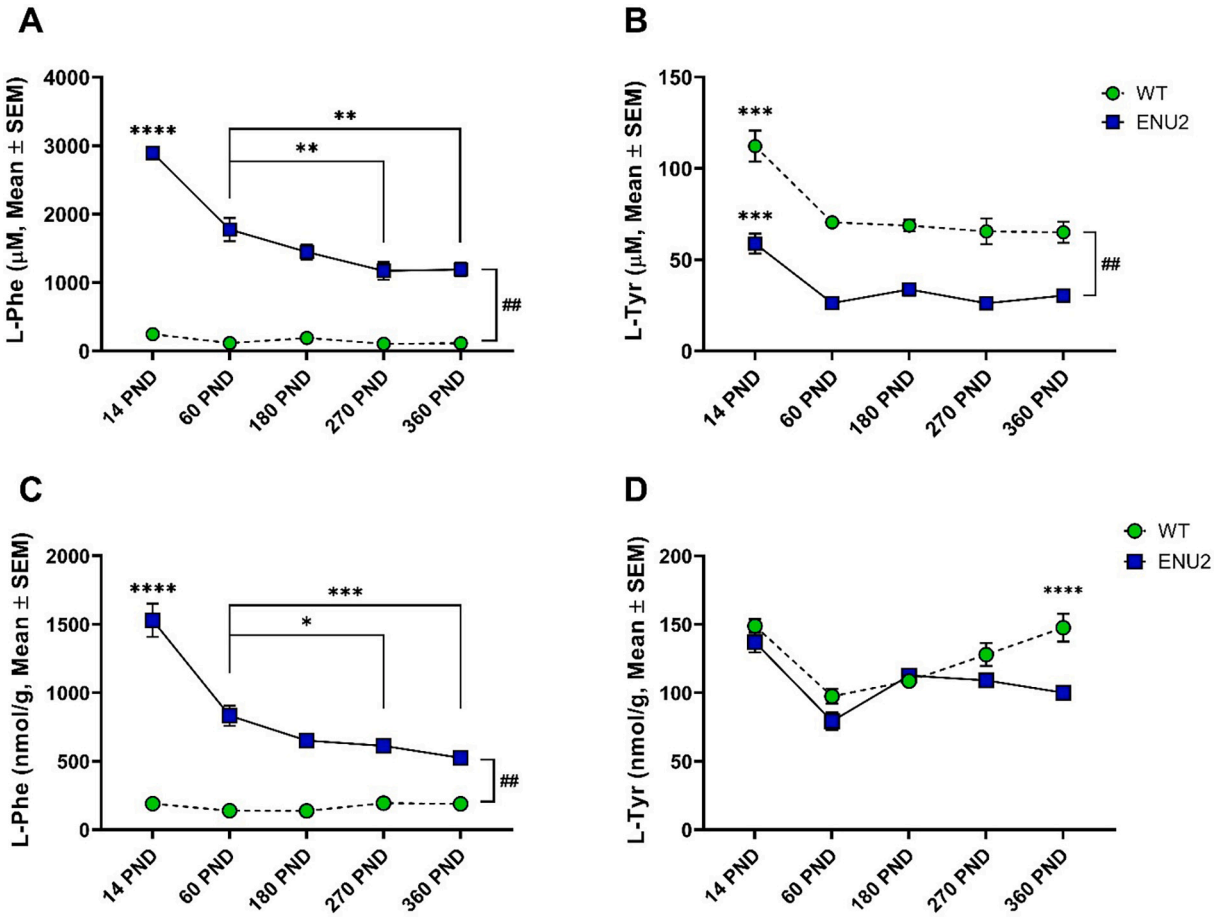

Fig. 2. (A) L-Phe concentration levels in WT and ENU2 bloostream. L-Phe concentration in ENU2 peripheral blood showed a progressive decrease during ENU2 mice lifespan. As expected, WT L-Phe was always lower compared to ENU2. (B) L-Tyr concentration levels in WT and ENU2 peripheral blood. Higher L-Tyr levels were detected at 14 PND in both conditions. As expected, L-Tyr was always lower in ENU2 mice compared to WT. Data are expressed as Mean ± SEM (WT 14 PND, WT $n = 3$, ENU2 $n = 11$; 60 PND, WT $n = 5$, ENU2 n = 5; 180 PND, WT $n = 4$, ENU2 n = 4; 270 PND, WT n = 5, ENU2 n = 5; 360 PND, WT n = 4, ENU2 $n = 6$). Two-way ANOVA followed by Bonferroni's multiple comparisons test, *p < 0.05; **$p < 0.01$; ***$p < 0.001$; ****p < 0.0001; ## p < 0.0001 WT vs ENU2 for each age. (C) L-Phe concentration levels in ENU2 and WT brains. L-Phe concentration in ENU2 brains showed a progressive decrease during ENU2 mice lifespan. As expected, WT L-Phe was always lower compared to ENU2. (D) L-Tyr concentration levels in ENU2 and WT brains. Unexpectedly, no statistically significant differences were detected between the two conditions, except for the time point 360 PND. Data are expressed as Mean ± SEM (WT 14 PND, WT n = 6, ENU2 n = 4; 60 PND, WT n = 5, ENU2 n = 4; 180 PND, WT n = 4, ENU2 n = 4; 270 PND, WT n = 5, ENU2 n = 5; 360 PND, WT n = 4, ENU2 n = 6). Two-way ANOVA followed by Bonferroni's multiple comparison test, ****p < 0.0001 for WT and ENU2 L-Tyr at 360 PND.

on RNA extracted from the same ENU2 and WT brain samples (see Table 1, *no 540 PND*) were performed. In contrast to what was expected, mRNA MBP was equally expressed in the two conditions in all the investigated times. Indeed, no significant differences were found, even if in the earlier time points considered (14-60-180 PND), MBP mRNA expression seems even to be higher in ENU2 compared to WT (Fig. 1E). These data, together with those obtained from WBs, suggest a possible impairment at the translational level during the first phases of development, which may result in the low MBP protein expression observed in ENU2 mice. As reported previously, MBP translation is a finely regulated process, and a disruption over the expression of cis- or trans-acting factors which regulate its translation could provoke a destabilization of the MBP translational process.

3.2. L-PHE levels in peripheral blood and brain decrease during ENU2 mice lifespan

In the peripheral blood, as expected, L-Phe levels in ENU2 mice for

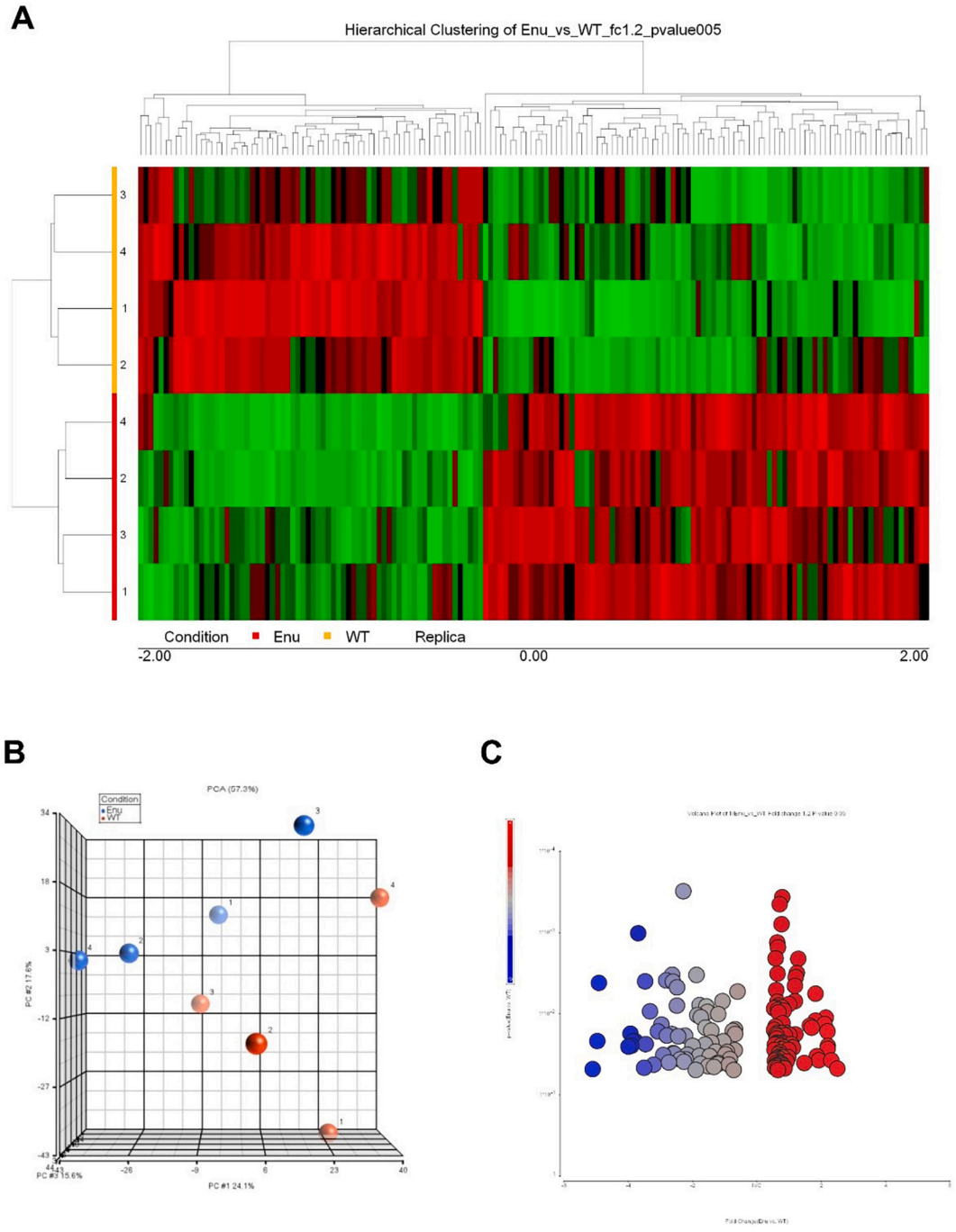

Fig. 3. Hierarchical clustering (A) analysis of differentially expressed microRNAs in WT ($n = 4$) and ENU2 (n = 4) mice brains with a fc > 1.2. 156 microRNAs were differentially expressed in ENU2 compared to WT mice, with statistical significance set at p-value: 0.05. Color gradation shows the relative expression of microRNAs: green, downregulation; red, upregulation. (B) PCA applied to the examinated samples, highlighting a certain degree of separation between the two conditions. Volcano plot (C) of differentially expressed microRNAs ENU2 and WT mice brains. Y-axis: p-value (0.05); X-axis: fold change (>1.2). Color gradation shows the relative expression of microRNAs: blue, downregulation; red, upregulation. (For interpretation of the references to color in this figure legend, the reader is referred to the web version of this article.)

all the intervals considered were significantly higher compared to WT mice (Fig. 2A, $^{\#\#}p < 0.0001$), while L-Tyr levels were significantly lower in ENU2 mice compared to WT (Fig. 2B, $^{\#\#}p < 0.0001$). As shown in Fig. 2A, L-Phe levels in the peripheral blood of ENU2 mice of 14 PND were significantly higher than any other time points. Levels of L-Phe remained higher until 60 PND with respect to those detected in the adult ENU2 animals aged 180 to 360 PND. Conversely, L-Tyr levels in ENU2 peripheral blood were persistently lower than in the control mice and declined with aging following the same trend observed in controls (Fig. 2B).

At cerebral level, as expected, L-Phe concentrations for all the intervals considered in ENU2 mice were significantly higher compared to the relative WT (Fig. 2C, $^{\#\#}p < 0.0001$), while the opposite was observed for L-Tyr concentrations, although significance was found only between WT and ENU2 brain L-Tyr levels at 360 PND (Fig. 2D, $^{\#\#}p < 0.0001$). Interestingly, as observed in the peripheral blood, L-Phe cerebral levels resulted in a decreasing trend during development in the ENU2 brain, with significantly higher levels detected at 14 PND compared to the other time points. L-Tyr, on the other hand, showed an unexpected fluctuating trend, with lower levels detected at 60 PND for both genetic conditions. L-Phe and L-Tyr concentrations values for both peripheral blood and brain are reported in Supplementary Material

Table 3
Differentially expressed proteins in the PKU mouse brain at 60 and 360 PND with fold > 1.5 and FDR < 0.1.

Accession	Description	Gene Symbol	Fold 60 PND	Fold 360 PND	Ratio P-Value 60 PND	Ratio P-Value 360 PND
		60 PND (ENU2/WT)				
Q9CXJ4	Mitochondrial potassium channel ATP-binding subunit	Abcb8	-1,52	1,03	3,04E-03	0,74
G5E895	Aldo-keto reductase family 1, member B10 (aldose reductase)	Akr1b10	-1,51	0,93	2,15E-06	0,65
E9Q804	Ankyrin repeat domain-containing protein 17	Ankrd17	-1,58	1,05	1,49E-02	0,72
Q8K298	Anillin	Anln	-1,68	1,04	7,33E-02	0,97
P14824	Annexin A6	Anxa6	-1,79	1,12	7,53E-02	0,89
Q8R3P0	Aspartoacylase	Aspa	-1,85	1,11	9,61E-08	0,33
P00920	Carbonic anhydrase 2	Car2	-1,55	1,05	2,01E-06	0,96
Q3TYV5	2′,3′-cyclic-nucleotide 3′-phosphodiesterase	Cnp	-1,52	1,07	2,29E-09	0,36
Q63870	Collagen alpha−1 (VII) chain	Col7a1	-1,59	0,98	4,57E-02	0,98
Q7TT37	Elongator complex protein 1	Elp1	-1,59	1,64	8,53E-03	4,82E-03
O35409	Glutamate carboxypeptidase 2	Folh1	-1,71	1,24	1,93E-02	0,59
Q3U011	GLTP domain-containing protein	Gltp	-1,72	1,04	2,25E-04	0,88
Q9QY42	Prosaposin receptor GPR37	Gpr37	-1,54	1,11	1,56E-02	0,83
P20917	Myelin-associated glycoprotein	Mag	-1,54	1,05	2,36E-07	0,73
P04370	Myelin basic protein	Mbp	-1,58	0,96	1,02E-06	1,00
Q61885	Myelin-oligodendrocyte glycoprotein	Mog	-1,66	1,09	1,07E-10	0,29
P60202	Myelin proteolipid protein	Plp1	-1,80	1,02	2,91E-10	0,82
Q91VC7	Protein phosphatase 1 regulatory subunit 14A	Ppp1r14a	-1,93	1,17	1,25E-09	0,23
P48379	DNA-binding protein RFX2	Rfx2	-1,87	0,94	9,77E-04	1,00
P50114	Protein S100-B	S100b	-1,91	0,93	1,23E-10	0,98
Q9D154	Leukocyte elastase inhibitor A	Serpinb1a	-1,60	1,15	2,05E-09	0,02
P31650	Sodium- and chloride-dependent GABA transporter 3	Slc6a11	-1,52	1,12	4,33E-07	0,33
B2RQX9	Sodium- and chloride-dependent glycine transporter 2	Slc6a5	-1,60	1,16	2,71E-03	0,66
P28571–1	Isoform GlyT-1A of sodium- and chloride-dependent glycine transporter 1	Slc6a9	-1,57	0,97	2,29E-03	0,99
D3YTU0	Vesicle-associated membrane protein 1	Vamp1	-1,57	1,03	1,33E-03	1,00
A0A0R4J2A2	Ankyrin repeat and sterile alpha motif domain-containing protein 1B	Anks1b	1,56	1,16	1,94E-02	0,96
P11798	Calcium/calmodulin-dependent protein kinase type II subunit alpha	Camk2a	1,57	1,13	1,25E-04	0,22
Q3UTQ8	Cyclin-dependent kinase-like 5	Cdkl5	1,62	1,19	1,78E-07	0,70
A0T1G3	C-type lectin domain family 1 member B	Clec1b	1,98	1,09	1,07E-02	0,74
Q3TY78	Guanine nucleotide-binding protein G(Olf) subunit alpha	Gnal	1,51	1,01	1,58E-04	0,70
Q542P2	Neuronal membrane glycoprotein M6-a	Gpm6a	1,53	0,87	1,78E-08	0,11
P39087	Glutamate receptor ionotropic, kainate 2	Grik2	1,50	0,92	1,77E-02	0,33
E9Q2Y3	NF-kappa-B essential modulator	Ikbkg	1,61	0,94	7,11E-03	0,48
Q3TZP3	Metastasis-associated protein MTA2	Mta2	1,77	0,95	7,94E-05	0,25
P60761	Neurogranin	Nrgn	1,63	1,17	2,97E-08	0,36
Q7TPG1	Phosphodiesterase	Pde10a	1,56	0,98	1,25E-02	0,87
S4R2S0	Piezo-type mechanosensitive ion channel component	Piezo2	1,50	0,91	2,91E-06	0,84
Q9D3P8	Plasminogen receptor (KT)	Plgrkt	1,52	1,01	5,77E-03	0,98
Q9QZC2	Plexin-C1	Plxnc1	1,61	0,98	1,35E-02	0,96
Q60829	Protein phosphatase 1 regulatory subunit 1B	Ppp1r1b	1,62	1,09	3,67E-09	0,54
E9PUC5	PH and SEC7 domain-containing protein 3	Psd3	1,52	0,97	6,13E-07	0,70
Q5U4D8	Sodium-dependent multivitamin transporter	Slc5a6	1,61	1,05	4,80E-02	0,95
Q9CY18	Sorting nexin-7	Snx7	1,58	1,12	1,63E-02	0,93
P11031	Activated RNA polymerase II transcriptional coactivator p15	Sub1	1,58	0,90	1,99E-11	0,09
Q3U336	Synaptopodin	Synpo	1,51	1,03	5,19E-05	1,00
Q99LG1	Transmembrane protein 51	Tmem51	1,50	1,10	1,85E-02	0,98
Q8K1S4	Netrin receptor UNC5A	Unc5a	1,66	1,25	1,20E-02	0,81
		360 PND (ENU2/WT)				
Q9D6E4	Tetratricopeptide repeat protein 9B	Ttc9b	1,29	-1,89	0,102	1,52E-03
P03995	Glial fibrillary acidic protein	Gfap	1,00	1,81	0,941	1,02E-07
P28665	Murinoglobulin-1	Mug1	0,95	2,15	0,987	7,06E-02
Q3TPW7	Phosphoglucomutase-2-Like 1	Pgm2l1	0,88	2,39	0,916	1,08E-04
P07758	Alpha-1-antitrypsin 1–1	Serpina1a	1,04	2,09	0,991	6,75E-04
P07759	Serine protease inhibitor A3K	Serpina3k	0,94	1,67	0,822	3,92E-02

Table 2.

3.3. miRNA microarray output analysis and miRNAs evaluation

Dobrowolski et al. (Dobrowolski et al., 2015, 2016) reported an important epigenetic remodeling in PKU patients and mice, which leads to the creation of hypo−/hypermethylated genomic loci and to the subsequent overexpression or downregulation of certain genomic elements such as miRNAs or lncRNAs. To verify if the MBP translation in ENU2 mice at late brain developmental stage could be impaired by miRNAs, total RNA samples from 60 PND WT and ENU2 mice (n = 4/condition) were analyzed through miRNA microarray technique. miRNA profiling for the differentially expressed miRNAs between the two conditions was depicted by hierarchical clustering (see Fig. 3A). PCA was applied in order to reduce complexity and maximize differences between the samples included in the study (Fig. 3B), revealing some level of separation between the two conditions under investigation. In fact, 156 miRNAs were found to be differentially expressed between WT and ENU2 mice after passing volcano plot filtering (fold change >1.2-fold, *p*-value <0.05; Fig. 3C). Of these 156 miRNAs, 68 were downregulated and 88 were upregulated in ENU2 mice compared to WT mice.

Target genes of the mature upregulated miRNAs with fc > 1.2 and mature downregulated miRNAs with fc > 2.5 were analyzed using target prediction bioinformatics tools (miRDB, TargetScanMouse 8.0 and DIANA TOOLS-microT-CDS), thus evaluating the possible molecular targets with the most promising scores in each of the mentioned tools. Only common target genes recognized by the three prediction tools (Supplementary Material Table 3) were considered for further analyses (GSEA - Supplementary Material Fig. S2A—B) and miRNAs-targets networks were built via Cytoscape software, highlighting proteins which could be targeted by more than one miRNA (Supplementary Material Fig. S3A—B). Interestingly, many miRNAs' targets resulted to be in common with two or more miRNAs, underlying their proximity and suggesting a possible mutual functionality.

The expression of 5 upregulated miRNAs (miR-671-3p, miR-217-5p, miR-448-5p, miR-218-1-3p and miR-1231-3p) were examined through RT-qPCR to validate miRNAs upregulation obtained from the microarray analysis. RT-qPCR results were analogous to those of the microarray analysis, even if statistical significance was recorded only for miR-217-5p (fc: 4.84), miR-218-1-3p (fc: 2.09) and miR-1231-3p (fc: 1.98) (data *not shown*).

3.4. Proteomic analyses outcome

In order to identify and evaluate candidate proteins which could be potential targets of the mature upregulated miRNAs and could interfere with the correct MBP translation, a proteomic analysis on WT and ENU2 brain lysates of 60 and 360 PND (n = 4/condition) using TMT quantification was performed, considering as differentially expressed proteins with a fold change 1.5 and FDR < 0.1. These two intervals (60–360 PND) were chosen following the MBP protein expression levels observed afterwards WB and IF analyses. The peptide labeling efficiency was about 90%, with 19.86% of labeled peptides which were filtered by isolation and thus not considered for the final evaluation. Moreover, the precursor contamination percentage was about 5%, with a good quality control after normalization of the ionic current signals (Supplementary Material Fig. S4A-B-C). Differentially expressed proteins with fc > 1.5 were evaluated after passing volcano plot filtering (Supplementary Material Fig. S5A—B) and PCA analysis was performed in order to highlight both samples variability and the relationship between WT and ENU2 brain proteins over the time points considered (60–360 PND) (Supplementary Material Fig. S5C).

As reported in Table 3, proteomic analysis detected 47 differentially expressed proteins between WT and ENU2 at 60 PND, with fold change set at 1.5 and FDR < 0.1. Of these proteins, 25 were significantly downregulated, while 22 were significantly upregulated in ENU2 compared to WT mice. Interestingly, many downregulated proteins at 60 PND normalized their own expression at 360 PND, thus highlighting the great cerebral plasticity already observed during MBP protein analyses. Speaking of MBP, its expression normalization in the middle-aged ENU2 mouse was confirmed also by the proteomic analysis; in fact, MBP raised from a ENU2/WT ratio of −1.639 at 60 PND to a ENU2/WT ratio of −1.052 at 360 PND, which is an indication of a complete normalization over protein expression during adulthood. Is also of note the protein expression recovery of many other myelin proteins, such as PLP1, MOG, CNP, and MAG (which increased from a fold of −1.54 at 60 PND to a fold of 1.05 at 360 PND). Moreover, protein expression normalization at 360 PND was observed also for other important downregulated proteins at 60 PND that are involved in myelin constitution, such as GPR37, VAMP1, ANLN, and ELP1 and for upregulated proteins at 60 PND which are involved as well in neuronal differentiation and migration (such as NRGN, STX7, GMP6A and SYNPO). At 360 PND, two protein were found significantly downregulated (TTC9B and ELP1), while 5 proteins were found significantly upregulated in ENU2 compared to WT (GFAP, MUG1, PGM2L1, SERPINA1A, SERPINA3K).

3.5. Bioinformatic analyses on up- and downregulated proteins

Proteomic results were bioinformatically analyzed in order to understand which relationships and/or pathways resulted to be altered in the late development of the ENU2 mice brain. Interactions between up- and downregulated proteins in ENU2 brain at 60 PND were analyzed after submission to the STRING database with a minimum required interaction score set to >0.40, while potential altered pathways were analyzed through gene set enrichment analysis. As reported in Fig. 4A, up- and downregulated myelin proteins are strictly interconnected, forming a significant cluster with a score of 4.154 comprehensive of 14 nodes and 27 edges. From gene set enrichment analysis (Fig. 4B-C-D), we found that significant up- and downregulated proteins are involved in many biological processes such as synaptic transmission, myelination, axon ensheathment and neurotransmitter uptake, while we found myelin sheath adaxonal region, dendritic spine, myelin sheath and presynaptic membrane among the possible altered cellular components. Lately, we also found that alterations on the structural constituent of myelin sheath, sodium symporter activity and protein serine/threonine phosphatase inhibitor activity can occur in the young ENU2 mouse brain.

3.6. miRNAs selection and relative validation of differentially expressed proteins

Proteomic analyses defined many downregulated proteins that could potentially be targets of the previously assessed upregulated miRNAs at 60 PND. In order to establish the most promising miRNA-protein relation that could explain the MBP trend observed during adulthood, and with the purpose to validate proteomic analyses, we decided to search for the common proteins among the potential upregulated miRNAs' targets and the downregulated proteins at 60 PND. Therefore, in this analysis, only the potential upregulated miRNAs detrimental effect was investigated, thus excluding the investigation for a possible relation between downregulated miRNAs and upregulated proteins in ENU2. To extend the research, we included in the analysis all the downregulated proteins with fold >1.2. As depicted from the Venn diagram in Fig. 5A, 14 proteins were in common between the two sets and thus were considered as potentially downregulated by the hindering action of the upregulated miRNAs (see Table 4).

Of the 14 candidate downregulated proteins, ANLN, MAG and CNTNAP2, which are potential targets for the significant upregulated miRNAs at 60 PND miR-217-5p, miR-218-1-3p and miR-1231-3p, respectively (Fig. 5B), were evaluated by western blot analyses. These proteins are, in fact, actively involved in the myelination process and their downregulation can lead to detrimental effects over myelin

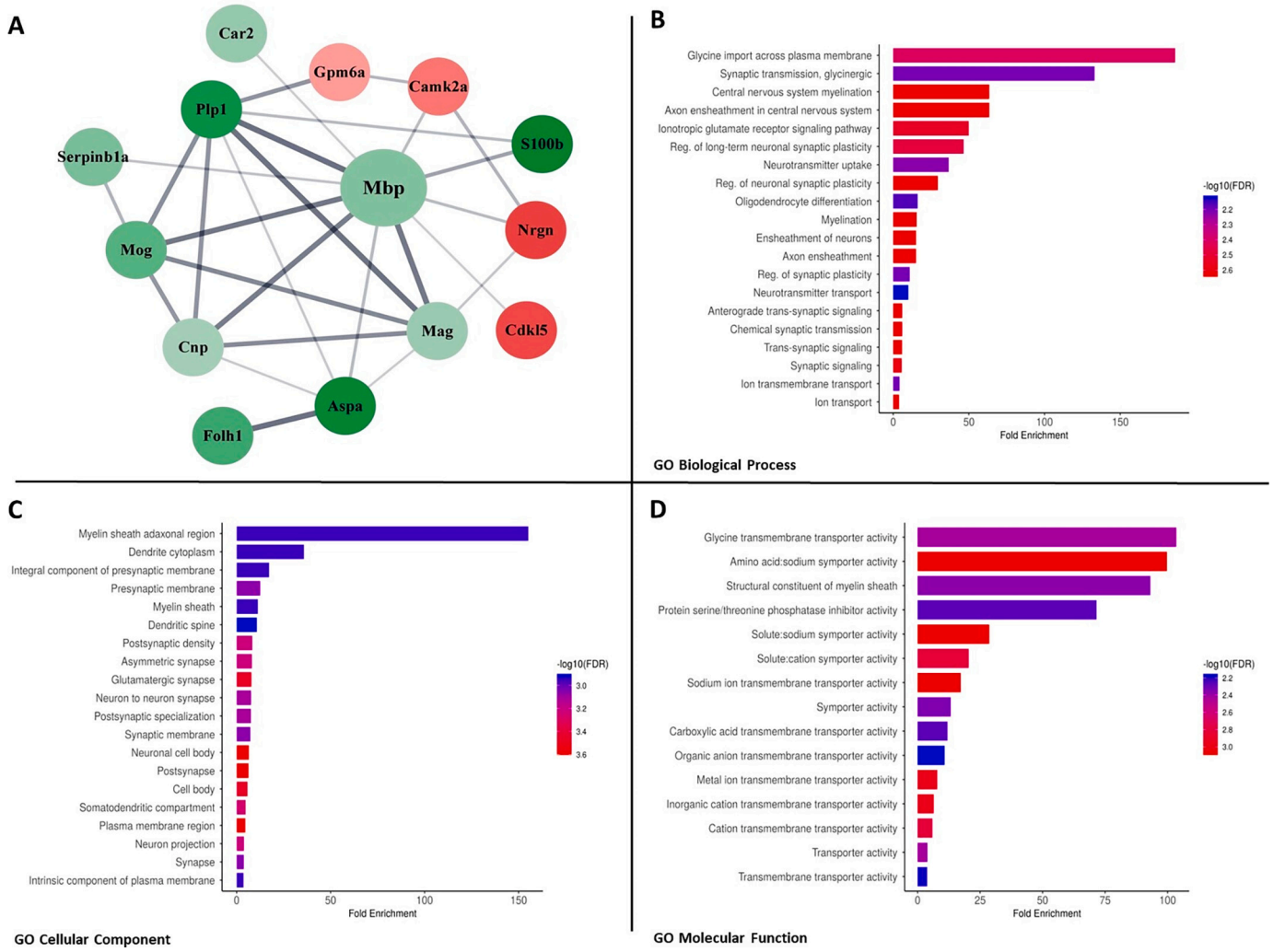

Fig. 4. (A) Up- and downregulated proteins in 60 PND ENU2 mouse brain forming a cluster of 14 nodes and 27 edges. The degree of up- or downregulation was reported as color gradient (green: downregulation; red: upregulation). (B-C-D) Gene Ontology for significant up- and downregulated protein at 60 PND (fold > 1.5). Enrichment analysis was performed for Biological Process (BP), Cellular Component (CC) and Molecular Function (MF). Fold Enrichment and FDR are reported. (For interpretation of the references to color in this figure legend, the reader is referred to the web version of this article.)

formation and scaffolding, as well as lower levels of MBP (Quarles, 2007; McKerracher and Rosen, 2015; Erwig et al., 2019; Scott et al., 2019). As reported in Fig. 5C-D-E, western blotting showed significant downregulation of ANLN and MAG proteins in the PKU mouse brain compared to the control ($p = 0.034$ and $p = 0.033$, respectively). CNTNAP2 was downregulated as well compared to WT mice, even though it resulted to be not significant using two-way ANOVA test ($p = 0.26$). At 360 PND all the three evaluated proteins normalized their own expression, confirming what was seen at the proteomic level.

3.7. miRNAs evaluation during ENU2 mice lifespan

The potential miRNAs that could be involved in the downregulation of the three proteins evaluated after proteomic and WBs (ANLN, MAG and CNTNAP2) were examined throughout mice lifespan, to assess if their expression was correlated with the corresponding target proteins levels and, consequently, to MBP levels. Therefore, we decided to evaluate miR-218-1-3p, miR-217-5p, miR-1231-3p and, together, the sncRNA715, which is described as one of the potential ncRNA that could regulate MBP correct protein synthesis (Bauer et al., 2012; Müller et al., 2015). As shown in Fig. 6, miRNAs' levels between WT and ENU2 mice fluctuated greatly in the time points considered, with a peak in correspondence of 60 PND and a declining trend along adulthood. miRNAs' expression was not as expected especially at 14 PND; however, at that age the L-Phe brain concentration was significantly higher compared to all the other time points considered, thus leading us to hypothesize another epigenetic reprogramming that could lead to new hyper- or hypomethylated loci in the ENU2 mice brains. These considerations may not be applied for miR-218-1-3p, because the expression of this miRNA at 14 PND was higher in ENU2 compared to WT, even though not significant (Fig. 6B—C). Concerning miR-218-1-3p, its trend is particularly interesting because its expression in ENU2 brains at 60 PND is significantly higher compared to the one found at 270 PND ($p = 0.0048$). The same consideration can be made for miR-1231-3p, since that its expression in young ENU2 brains is higher compared to the one found at 270 and 360 PND ($p = 0.0022$ and $p = 0.008$, respectively). Moreover, although its low expression in ENU2 at 14 PND, miR-217-5p should be considered as a promising miRNA because its expression at 60 PND is significantly increased compared to all the other intervals of time (ENU2 60 PND vs 14 PND: $p < 0.0001$; ENU2 60 PND vs 180 PND: $p = 0.0002$; ENU2 60 PND vs 270 PND: $p < 0.0001$; ENU2 60 PND vs 360 PND: $p = 0.0022$) (Fig. 6A). Finally, sncRNA715 was not considered as the potential cause of MBP detrimental translation, since that was lower in ENU2 brains and its trend did not follow the one observed for MBP (Fig. 6D). Surprisingly, 2 out of the 3 miRNAs evaluated during mice lifespan (miR-217-5p and -218-1-3p) showed a mild increasing trend on

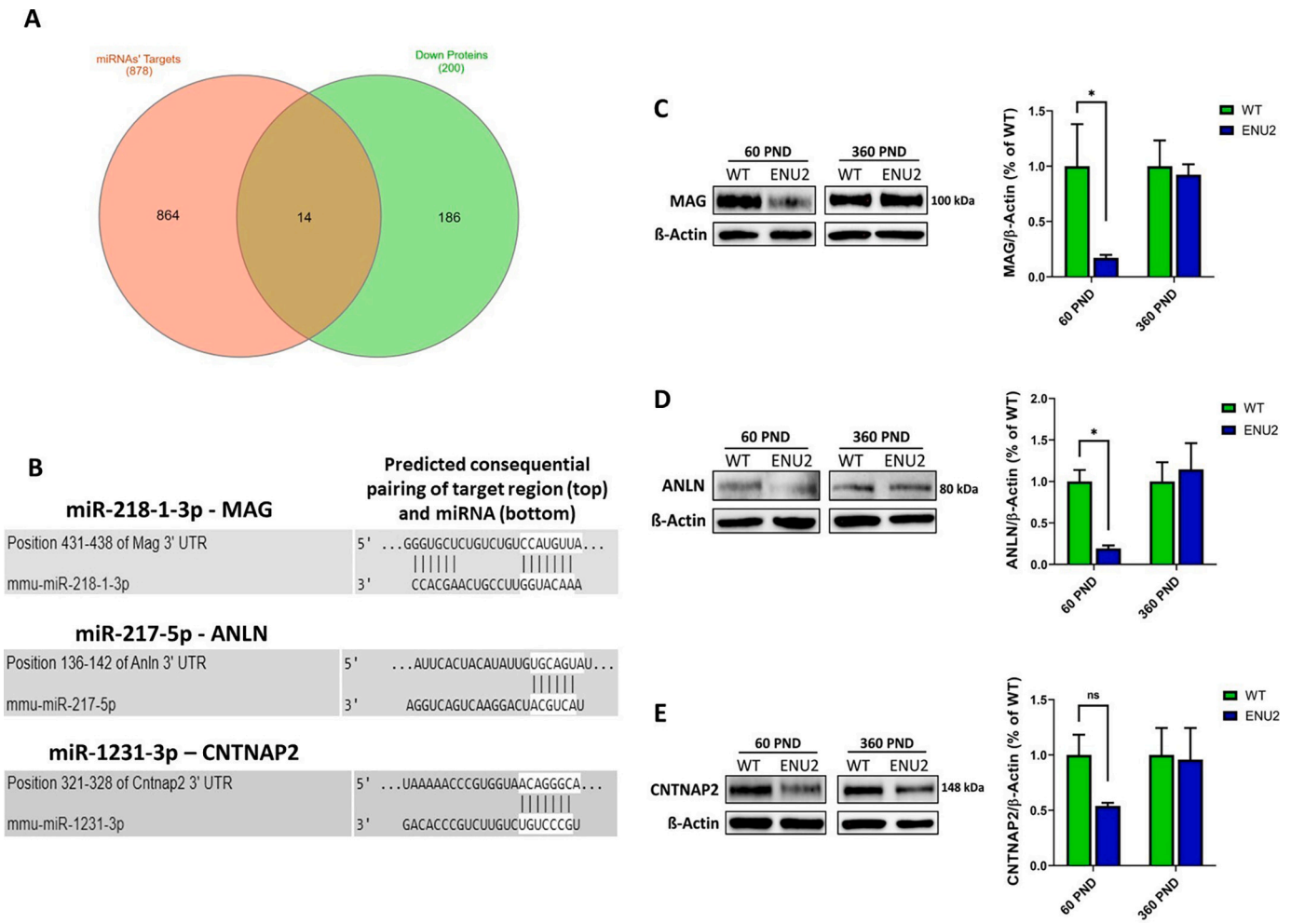

Fig. 5. (A) Venn diagram between mature upregulated (fc > 1.2) miRNAs' targets (in red) and downregulated proteins (fold >1.2) at 60 PND (in green). 14 downregulated proteins were in common between the two sets, suggesting the potential inhibitory action of upregulated miRNAs on their expression. (B) Predicted consequential pairing of target region (top) and miRNA (bottom) for the three significant upregulated miRNAs (miR-218-1-3p, miR-217-5p, miR-1231-3p) and the respective predicted targets. Image taken from TargetScanMouse 8.0. Representative immunoblots and densitometric analysis of (C) MAG, (D) ANLN and (E) CNTNAP2 showing the expression levels of the proteins in WT and ENU2 brains at 60 and 360 PND. The evaluated proteins showed depressed expression in ENU2 mice brains at 60 PND, recovering, with a normalization at 360 PND. Data are expressed as Mean ± SEM ($n = 4$/condition). All the reported values in the graph are densitometric values obtained using Image Lab software. Two-way ANOVA followed by Bonferroni's multiple comparison test, $^*p < 0.05$. (For interpretation of the references to color in this figure legend, the reader is referred to the web version of this article.)

their expression in ENU2 mice of 360 PND, which however may be due mostly to aging (Smith-Vikos and Slack, 2012; Noren Hooten et al., 2013) rather than diverse L-Phe levels.

4. Discussion

Hypomyelination and gliosis in the CNS could represent one of the possible explanations for the neuropathological background of neurodevelopmental derangement and neurological impairment observed in untreated PKU patients and in preclinical models of the disease. In rodents, myelination completes its processes after ≈ 30 days of age (Norton and Poduslo, 1973) and, in the same period, the brain of PKU mice is exposed to a relevant amount of blood L-Phe concentration that leads to an alteration of myelinated axons, as observed in hypomyelinated areas of mutant animals (Shefer et al., 2000). MBP, the second most abundant protein of the CNS myelin, plays a crucial role in myelination and it is essential for the assembly of a mature and functioning myelin membrane (Boggs et al., 1986; Campagnoni and Macklin, 1988; Nave and Werner, 2014). MBP protein expression is found to be altered in frontal cortex and striatum of adult untreated PKU mice and rat, with a recovery after a 4-week L-Phe restricted diet (Burri et al., 1990; Joseph and Dyer, 2003; Pascucci et al., 2018). To contribute to this topic, we explored MBP protein and MBP mRNA expression levels in the brain of young and fully grown ENU2 mice. Myelin PLP1 protein levels were also evaluated from 14 to 60 PND. WBs followed by densitometric analyses revealed that MBP protein is lower in young ENU2 mice compared to WT, confirming previous data obtained by Pascucci et al. (Pascucci et al., 2018). Interestingly, MBP recovered itself to nearly normal levels in middle- and aged ENU2 mice. Confocal analysis of immunofluorescence material as well confirmed the MBP expression recovery in later PND times. To date, this observation on the expression of MBP in the adult mouse constitutes a novel finding and it would be consistent with the delayed myelination detected in biochemically generated hyperphenylalaninemic rats (Baba et al., 1987; Burri et al., 1990). So far, there are no available data about middle-aged PKU rodents that could illustrate a possible cognitive recovery after MBP increasing. In any case, on clinical ground, untreated adult mice with PKU are clinically impaired and no improvement may be detected without treatment (Winn et al., 2022). However, this is not in contrast with the possible pathogenetic role of MBP defect since it happens during a critical stage of postnatal CNS maturation, thus potentially affecting the normal development of brain connectivity. One possible explanation that could elucidate the

Table 4
Potential relation between mature upregulated miRNAs' (fc > 1.2) targets and downregulated proteins at 60 PND (fold >1.2) in ENU2 brains.

miRNA name	Fold change ENU2 vs WT (RT-qPCR fold change)	Downregulated targets at 60 PND (fold change)	Description
miR-218-1-3p	2.14 (2.09)	**MAG (−1.54)**	**myelin-associated glycoprotein [Source:MGI Symbol;Acc: MGI:96912]**
		ANKRD29 (−1.25)	ankyrin repeat domain 29 [Source:MGI Symbol;Acc: MGI:2687055]
miR-217-5p	2.07 (4.84)	**ANLN (−1.68)**	**anillin, actin binding protein [Source:MGI Symbol;Acc: MGI:1920174]**
miR-185-3p	1.9	ADD1 (−1.33)	adducin 1 (alpha) [Source: MGI Symbol;Acc:MGI:87918]
		PHLDB1 (−1.31)	pleckstrin homology like domain, family B, member 1 [Source:MGI Symbol;Acc: MGI:2143230]
miR-1231-3p	1.77 (1.98)	**CNTNAP2 (−1.21)**	**contactin associated protein-like 2 [Source:MGI Symbol;Acc: MGI:1914047]**
miR-6923-3p	1.52	ERMN (−1.47)	ermin, ERM-like protein [Source:MGI Symbol;Acc: MGI:1925017]
miR-135a-1-3p	1.41	SNX32 (−1.23)	sorting nexin 32 [Source:MGI Symbol;Acc: MGI:2444704]
miR-6989-3p	1.33	SLC16A1 (−1.31)	solute carrier family 16, member 1 [Source:MGI Symbol;Acc: MGI:106013]
miR-93-3p	1.3	PHLDB1 (−1.31)	pleckstrin homology like domain, family B, member 1 [Source:MGI Symbol;Acc: MGI:2143230]
		RAP1A (−1.22)	RAS-related protein 1a [Source:MGI Symbol;Acc: MGI:97852]
miR-672-5p	1.29	LAMP5 (−1.42)	lysosomal-associated membrane protein family, member 5 [Source:MGI Symbol;Acc:MGI:1923411]
		ANK1 (−1.22)	ankyrin 1, erythroid [Source:MGI Symbol;Acc: MGI:88024]
miR-540-3p	1,26	SLC25A5 (−1.25)	solute carrier family 25, member 5 [Source:MGI Symbol;Acc: MGI:1353496]
miR-763	1.25	NAT8L (−1.29)	*N*-acetyltransferase 8-like [Source:MGI Symbol;Acc: MGI:2447776]
miR-874-3p	1.25	CNTNAP2 (−1.21)	contactin associated protein-like 2 [Source:MGI Symbol;Acc: MGI:1914047]

lower MBP protein levels observed during early development lies on a diminished brain large neutral amino acids (LNAAs) availability due to high L-Phe levels, which in turn may lead to an impaired protein synthesis (Hoeksma et al., 2009; de Groot et al., 2013, 2015). At this point, it is important to clarify that brain dysfunctions observed in PKU patients and animal models can not be accounted only over L-Phe toxicity (van Spronsen, 2009); in fact, the L-Phe excess can indirectly lead to a decreased functionality of the enzymes tyrosine hydroxylase and tryptophan hydroxylase, leading to lower levels of the neurotransmitters dopamine and serotonine, respectively (Winn, 2016, 2018). Moreover, L-Phe higher levels alone do not completely correlate with LNAAs shortage, which in turn, as reported before, is held to be the cause of the lower protein synthesis detected in PKU mouse (Hoeksma et al., 2009; van Spronsen et al., 2021). Nonetheless, our previous work (Pascucci et al., 2018) reported that, along with MBP reduction, neurofilament light polypeptide (NFL) expression was unaltered in ENU2 mice at 60 PND, while - in the current work - a slight decrease was detected in Myelin PLP1 protein levels in ENU2 mice brains at 14–60 PND, thus suggesting a possible severe hindrance only over MBP expression. Further, mRNA expression revealed no significant changes at the time points considered, with a tendency to be more expressed in the first months of life in ENU2 mice. Together, MBP mRNA and Myelin PLP1 data obtained are consistent with the assessments made by Schoemans and colleagues (Schoemans et al., 2010) and could pave the way to the hypothesis of an impaired MBP translation during the first months of life. Several studies report that MBP mRNA translation does not occur immediately but is regulated locally and temporally by ribonucleoproteins (i.e. hnRNP-K and hnRNP-A2) (Laursen et al., 2011; Müller et al., 2013; Torvund-Jensen et al., 2014), kinases (i.e. ERK2 and FYN) (White et al., 2008; Michel et al., 2015), and a small non-coding RNA (sncRNA715, (Bauer et al., 2012; Müller et al., 2015)) that allow MBP translation only once it has reached the plasma membrane through RNA granules. Previous studies by Dobrowolski et al. revealed altered DNA methylation patterns associated with high levels of blood L-Phe in the PAH^{Enu2} brain tissue (as well as in the brain of two adult PKU patients) that could provoke an alteration of genomic elements such as lnRNAs and miRNAs (Dobrowolski et al., 2015, 2016). Although the molecular mechanism by which L-Phe can modify brain epigenome remains elusive, the study conducted by Dobrowolski et al. pointed out that animals undergoing L-Phe restricted diet displayed an attenuated pattern of aberrant DNA methylation compared to hyperphenylalaninemic mice, thus emphasizing the brain epigenome repatterning as one of the possible response to toxic L-Phe exposure (Dobrowolski et al., 2016). Following these assumptions, we probed the possibility that these modifications may be implied in the pathogenesis of MBP translational deficit by designing a long-term study in the ENU2 mice. Firstly, to evaluate if MBP upward trend and the potential presence of differentially expressed miRNAs were connected by diverse L-Phe concentrations, L-Phe levels were measured in WT and ENU2 mice from 14 to 360 PND. The obtained results showed an unprecedented significant blood L-Phe levels decline during aging in ENU2 mice, which nonetheless could be consistent with the decreasing tendency observed in our previous work from 15 to 70 PND (Pascucci et al., 2018). Likewise, a remarkable reduction of L-Phe concentration was also found in ENU2 brains from 14 to 360 PND. This trend is possibly related to a residual activity of the PAH enzyme (Hamman et al., 2005), which could be driven by developmental patterns. Notably, the 3-times L-Phe reduction from 14 to 360 PND in the ENU2 brains observed in this work appears to be sufficient to revert MBP expression, similarly to what reported by Joseph and Dyer with ENU2 mice submitted to low L-Phe diet on the first week (Joseph and Dyer, 2003). Taken together, our results support the hypothesis that in the first months of life of the ENU2 mice some epigenetic alterations (i.e. differentially expressed miRNAs or ncRNAs), connected with the increase of the brain L-Phe, may disturb MBP translational process, leading to low MBP expression. In fact, miRNA microarray analysis carried out on ENU2 and WT mice brains of 60 PND revealed that 156 miRNAs were differentially expressed in ENU2 mice compared to WT. This analysis was followed by gene set enrichment analysis on mature up- and downregulated miRNAs' targets (fc > 1.2 and fc > 2.5, respectively), which showed that many neuronal pathways could be altered in ENU2 mice brains. Unfortunately, using prediction tools with high scores, none of the detected upregulated miRNAs has MBP among its potential targets, nor has the MBP regulatory elements mentioned before. Nonetheless, in order to confirm the in silico predictive hypotheses and to point out which miRNA could have an indirect impact over MBP correct translation, we analyzed the total

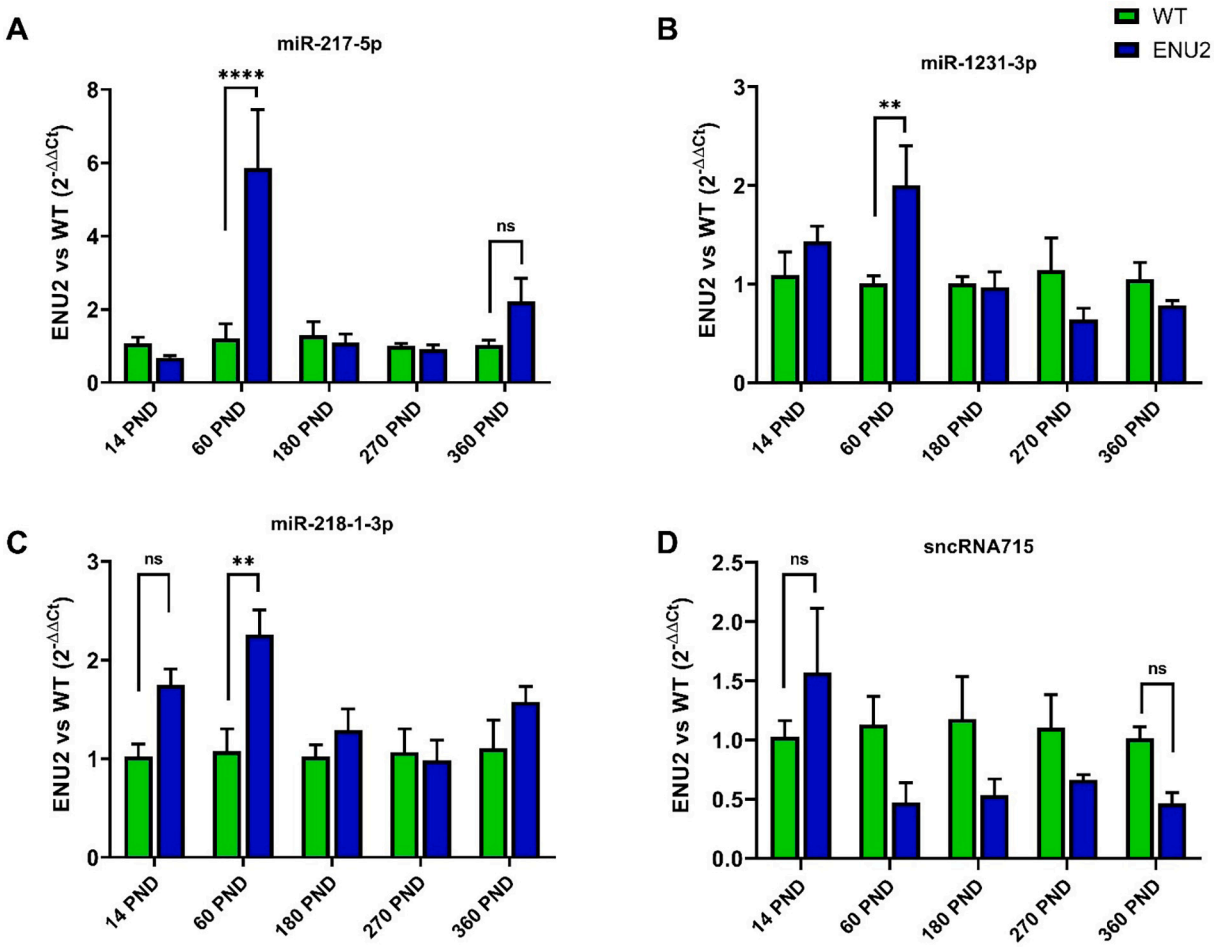

Fig. 6. (A) miR-217-5p, (B) miR-1231-3p, (C) miR-218-1-3p and (D) sncRNA715 expression profiling during mice lifespan. Higher miRNAs expression leves were detected in ENU2 brains of 60 PND compared to WT. Data were analyzed through RT-qPCR and presented as $2^{-\Delta\Delta CT}$ relative to the levels of WT miRNAs expression. Data are expressed as Mean ± SEM (n = 4/group). Total RNA was extracted from the same 4 animals/condition evaluated in the proteomic assay. snoRNA202 was used as endogenous small non-coding RNA. Two-way ANOVA followed by Tukey's multiple comparison test, *p < 0.05; **$p < 0.01$; ***$p < 0.001$; ****$p < 0.0001$.

proteome of ENU2 mice brains of 60 and 360 PND through proteomic assay, with ENU2/WT fold >1.5. Proteomic analyses reported a general normalization of brain proteins at 360 PND, confirming the retrieved protein expression observed for MBP. Apart from MBP, among the downregulated proteins we found PLP1 (which strengthens the decrease observed in WB and IF), MOG, CNP, MAG and MOBP (the latter was not significant), all proteins involved in oligodendrocytes development, correct myelination and neuronal extracellular signaling (Solly et al., 1996; Quarles, 2007; Cloake et al., 2018). The general lower level of myelin proteins observed in ENU2 brains could be explained by many assumptions, going from widespread demyelination to astrocyte cell death induced by high L-Phe levels (Gregg et al., 2009; Preissler et al., 2016; Thau-Zuchman et al., 2022). Even so, given the protein recovery and the lower levels of peripheral blood and cerebral L-Phe at 360 PND, we decided to move forward on the epigenetic remodeling hypothesis throughout lifetime (Dobrowolski et al., 2015, 2016), evaluating the potential miRNAs that could indirectly affect myelin formation and, consequently, MBP expression in the young ENU2 mice (Stadelmann et al., 2019). To do so, we merged all the downregulated proteins at 60 PND (increasing the pool to the proteins with fold >1.2) with the upregulated miRNAs' targets (fc > 1.2), obtaining 14 candidate proteins that could be potentially affected by miRNAs' higher expression. Among them, we selected and validated by WBs 3 downregulated proteins in ENU2 at 60 PND that could be targeted by the upregulated miRNAs: ANLN, MAG and CNTNAP2. ANLN is fundamental in the correct myelin folding and its downregulation leads to the disruption of myelin septin assembly and consequently to pathological myelin outfoldings (Patzig et al., 2016; Erwig et al., 2019). This protein is potentially targeted by miR-217-5p, which is significantly upregulated at 60 PND; notably, miR-217-5p – ANLN relationship was already been observed by Idichi et al. (Idichi et al., 2017), thus confirming the possible detrimental activity of miR-217-5p on ANLN correct expression. On the other hand, MAG is strictly associated with MBP (Mann et al., 2008; Cheishvili et al., 2014) and its downregulation or deletion can provoke demyelination and white matter damages similar to what observed for multiple sclerosis (Quarles, 2007; Rahmanzadeh et al., 2018). Moreover, MAG as been reported as the key transmembrane protein that activates Fyn-kinase in the initial events of myelination (Umemori et al., 1994; White et al., 2008), which in turn phosphorylates several components of the MBP and MOBP mRNA granule, finally allowing the release of MBP mRNA from its inhibitors and its subsequent localized translation (Schäfer et al., 2016). Activation via Fyn kinase is indeed crucial during the MBP translational process, given that MBP levels are reduced in Fyn-knockout mice (Umemori et al., 1999; Lu et al., 2005; White et al., 2008). In our case, MAG is potentially targeted by miR-218-1-3p, which is particularly interesting because its expression follows an opposite trend compared to MBP expression. From our analyses we also detected a downregulation of CNTNAP2, which can cause defective neurotransmission, developmental delay in cortical neurons and a decreased MBP expression (Scott et al., 2019; Lu et al., 2021). In this case, the protein could be a potential target for miR-1231-3p, which, similarly to miR-218-1-3p, shows an opposite trend compared to MBP during ENU2

mice lifespan. Finally, is of note the downregulation of ERMN, potentially mediated by the action of miR-6923-3p (microarray fc: 1.52). In fact, this protein is fundamental in the cytoskeletal rearrangements during the late wrapping and it plays an important role in the maintenance and stability of myelin sheath in the adult (Brockschnieder et al., 2006; Wang et al., 2020). Moreover, knockout of ERMN leads to lower MBP levels and to an aberrant myelin architecture (Wang et al., 2020; Ziaei et al., 2022). Taken together, the upregulation of the previously discussed miRNAs during early and late brain development may have a detrimental effect on the expression of target proteins that are involved in the MBP efficient translation (Bijlard et al., 2015; Stadelmann et al., 2019). These findings give a brand-new possible explanation for the depressed MBP expression observed in the young ENU2 mice, taking into account for the first time the potential activity of miRNAs over MBP correct regulation.

5. Conclusions

In summary, our studies confirm the MBP impairment in the first months of the ENU2 mouse brain development, together with a progressive recovery of MBP expression in the adult and aged ENU2 mouse. At the same time, MBP mRNA expression levels were found to be unaltered between ENU2 and WT, thus excluding a regulation mechanism at the transcriptional level and suggesting translational or post-translational regulation. In this scenario, miRNAs can have a key role, as we found miR-218-1-3p, miR-1231-3p and miR-217-5p to be potentially involved in the decreased MBP translation observed for the young ENU2 mouse brain. These observations are novel and can contribute to enhance the knowledge over MBP regulation and, overall, over PKU neurological outcomes, linking the epigenetic modifications data with the miRNAs' differential expression highlighted in this work. In fact, since that multiple possible miRNAs' targets for the detected differentially expressed miRNAs belong to the neuronal network, an altered expression of target genes caused by miRNAs activity could have detrimental effects on CNS development. Nonetheless, despite being promising, the relationship between epigenetic modifications and miRNAs' altered expression remains unclear, with brain chromatin immunoprecipitation (ChIP) analysis that could be fundamental to link the hyper- or hypomethylated loci with the differentially expressed miRNAs. Still, these findings need to be addressed with further investigations (i.e. with cellular models or lowering the target prediction score) in order to validate the hypotheses made, also verifying their evolution in aged ENU2 mice. Moreover, further studies will be necessary in order to assess if MBP increasing could lead to cognitive and/or myelination retrieval and if MBP could recover itself after selective antisense miRNAs administration. Finally, brain and blood metabolites and/or markers between 60 and 360 PND ENU2 mice will be also needed in order to check if some proteins (i.e. hormones) or metabolites are involved in the L-Phe lower levels observed in aged ENU2 peripheral blood and brain and, consequently, in the PKU cerebral outcome.

Funding

This work was partially supported by EryDel SpA and with the financial assistance of the European Union POR MARCHE FESR 2014/2020. Asse 1, OS 2, Azione 2.1-Intervento 2.1.1-Sostegno allo sviluppo di una piattaforma di ricerca collaborativa negli ambiti della specializzazione intelligente. Thematic Area: “Medicina personalizzata, farmaci e nuovi approcci terapeutici.” Project acronym: Marche BioBank www.marchebiobank.it.Marche BioBank research platform (POR MARCHE FESR 2014/2020).

CRediT authorship contribution statement

Alessandro Bregalda: Conceptualization, Validation, Investigation, Methodology, Visualization, Formal analysis, Data curation, Writing – original draft. **Claudia Carducci:** Methodology, Investigation, Data curation. **Maria Teresa Viscomi:** Methodology, Investigation, Data curation, Writing – review & editing. **Francesca Pierigè:** Methodology, Investigation. **Sara Biagiotti:** Writing - Review & Editing. **Michele Menotta:** Methodology, Investigation, Data Curation, Writing - Review & Editing. **Federica Biancucci:** Methodology, Investigation. **Tiziana Pascucci:** Writing – review & editing. **Vincenzo Leuzzi:** Writing – review & editing. **Mauro Magnani:** Writing – review & editing, Supervision, Resources, Project administration, Funding acquisition. **Luigia Rossi:** Conceptualization, Writing – review & editing, Supervision, Resources, Project administration, Funding acquisition.

Declaration of Competing Interest

Mauro Magnani and Luigia Rossi hold shares in EryDel SpA, a company with interests in the technology of RBC-based drug delivery. The other authors declare that the research was conducted in the absence of any commercial or financial relationships that could be construed as a potential conflict of interest.

Data availability

All data generated or analyzed during this study are included in this published article (and its Supplementary Material files) and available from the corresponding author on reasonable request.

Acknowledgments

Authors would like to thank Dr. Claudia Scopa for animal shelter management and animal care supervision. Authors would also like to thank Dr. Simone Minardi (IFOM-IEO Campus, Milan) for carrying out the miRNA microarray analysis.

Appendix A. Supplementary data

Supplementary data to this article can be found online at https://doi.org/10.1016/j.nbd.2023.106093.

References

Agarwal, V., et al., 2015. Predicting effective microRNA target sites in mammalian mRNAs. Elife 4, e05005. https://doi.org/10.7554/eLife.05005.
Anderson, P.J., Leuzzi, V., 2010. White matter pathology in phenylketonuria. Mol. Genet. Metab. 99 (Suppl. 1), S3–S9. https://doi.org/10.1016/j.ymgme.2009.10.005.
Andolina, D., et al., 2011. 5-Hydroxytryptophan during critical postnatal period improves cognitive performances and promotes dendritic spine maturation in genetic mouse model of phenylketonuria. Int. J. Neuropsychopharmacol. 14 (4), 479–489. https://doi.org/10.1017/S1461145710001288.
Baba, H., et al., 1987. Developmental changes of myelin-associated glycoprotein in rat brain: study on experimental hyperphenylalaninemia. Neurochem. Res. 12 (5), 459–463. https://doi.org/10.1007/BF00972298.
Bader, G.D., Hogue, C.W.V., 2003. An automated method for finding molecular complexes in large protein interaction networks. BMC Bioinform. 4 (1), 2. https://doi.org/10.1186/1471-2105-4-2.
Bale, T.L., 2015. Epigenetic and transgenerational reprogramming of brain development. Nat. Rev. Neurosci. 16 (6), 332–344. https://doi.org/10.1038/nrn3818.
Baron, W., et al., 2015. The major myelin-resident protein PLP is transported to myelin membranes via a transcytotic mechanism: involvement of sulfatide. Mol. Cell. Biol. 35 (1), 288–302. https://doi.org/10.1128/MCB.00848-14.
Bartel, D.P., 2004. MicroRNAs: genomics, biogenesis, mechanism, and function. Cell 116 (2), 281–297. https://doi.org/10.1016/s0092-8674(04)00045-5.
Bauer, N.M., et al., 2012. Myelin basic protein synthesis is regulated by small non-coding RNA 715. EMBO Rep. 13 (9), 827–834. https://doi.org/10.1038/embor.2012.97.
Baumann, N., Pham-Dinh, D., 2001. Biology of oligodendrocyte and myelin in the mammalian central nervous system. Physiol. Rev. 81 (2), 871–927. https://doi.org/10.1152/physrev.2001.81.2.871.
Bijlard, M., et al., 2015. Transcriptional expression of myelin basic protein in oligodendrocytes depends on functional syntaxin 4: a potential correlation with autocrine signaling. Mol. Cell. Biol. 35 (4), 675–687. https://doi.org/10.1128/MCB.01389-14.
Boggs, J.M., 2006. Myelin basic protein: a multifunctional protein. Cell. Mol. Life Sci. 63 (17), 1945–1961. https://doi.org/10.1007/s00018-006-6094-7.

Boggs, J.M., et al., 1986. Interaction of myelin basic protein with different ionization states of phosphatidic acid and phosphatidylserine. Chem. Phys. Lipids 39 (1–2), 165–184. https://doi.org/10.1016/0009-3084(86)90110-6.
Bortoluzzi, V.T., et al., 2021. Oxidative stress in phenylketonuria-evidence from human studies and animal models, and possible implications for redox signaling. Metab. Brain Dis. 36 (4), 523–543. https://doi.org/10.1007/s11011-021-00676-w.
Brockschnieder, D., et al., 2006. Ermin, a myelinating oligodendrocyte-specific protein that regulates cell morphology. J. Neurosci. 26 (3), 757–762. https://doi.org/10.1523/JNEUROSCI.4317-05.2006.
Burri, R., et al., 1990. Brain damage and recovery in hyperphenylalaninemic rats. Dev. Neurosci. 12 (2), 116–125. https://doi.org/10.1159/000111840.
Campagnoni, A.T., Macklin, W.B., 1988. Cellular and molecular aspects of myelin protein gene expression. Mol. Neurobiol. 2 (1), 41–89. https://doi.org/10.1007/BF02935632.
Campagnoni, A.T., et al., 1993. Structure and developmental regulation of Golli-mbp, a 105-kilobase gene that encompasses the myelin basic protein gene and is expressed in cells in the oligodendrocyte lineage in the brain. J. Biol. Chem. 268 (7), 4930–4938.
Carducci, C., et al., 1996. Automated method for the measurement of amino acids in urine by high-performance liquid chromatography. J. Chromatogr. A 729 (1–2), 173–180. https://doi.org/10.1016/0021-9673(95)00964-7.
Chace, D.H., et al., 1993. Rapid diagnosis of phenylketonuria by quantitative analysis for phenylalanine and tyrosine in neonatal blood spots by tandem mass spectrometry. Clin. Chem. 39 (1), 66–71.
Cheishvili, D., et al., 2014. IKAP deficiency in an FD mouse model and in oligodendrocyte precursor cells results in downregulation of genes involved in oligodendrocyte differentiation and myelin formation. PLoS One 9 (4), e94612. https://doi.org/10.1371/journal.pone.0094612.
Chen, Y., Wang, X., 2020. miRDB: an online database for prediction of functional microRNA targets. Nucleic Acids Res. 48 (D1), D127–D131. https://doi.org/10.1093/nar/gkz757.
Cloake, N.C. et al., 2018. PLP1 mutations in patients with multiple sclerosis: identification of a new mutation and potential pathogenicity of the mutations. J. Clin. Med. 7(10). doi: https://doi.org/10.3390/jcm7100342.
Dobrowolski, S.F., et al., 2015. Altered DNA methylation in PAH deficient phenylketonuria. Mol. Genet. Metab. 115 (2), 72–77. https://doi.org/10.1016/j.ymgme.2015.04.002.
Dobrowolski, S.F., et al., 2016. DNA methylation in the pathophysiology of hyperphenylalaninemia in the PAH(enu2) mouse model of phenylketonuria. Mol. Genet. Metab. 119 (1–2), 1–7. https://doi.org/10.1016/j.ymgme.2016.01.001.
Dobrowolski, S.F., et al., 2022. Comparative metabolomics in the Pahenu2 classical PKU mouse identifies cerebral energy pathway disruption and oxidative stress. Mol. Genet. Metab. 136 (1), 38–45. https://doi.org/10.1016/j.ymgme.2022.03.004.
Dyer, C.A., et al., 1996. Evidence for central nervous system glial cell plasticity in phenylketonuria. J. Neuropathol. Exp. Neurol. 55 (7), 795–814. https://doi.org/10.1097/00005072-199607000-00005.
Erwig, M.S., et al., 2019. Anillin facilitates septin assembly to prevent pathological outfoldings of central nervous system myelin. Elife 8. https://doi.org/10.7554/eLife.43888.
Fu, Y., et al., 2019. Recent progress in microRNA-based delivery systems for the treatment of human disease. ExRNA 1 (1), 24. https://doi.org/10.1186/s41544-019-0024-y.
Galloway, D.A., Moore, C.S., 2016. miRNAs as emerging regulators of oligodendrocyte development and differentiation. Front. Cell Dev. Biol. 4, 59. https://doi.org/10.3389/fcell.2016.00059.
Gandhi, R., 2015. miRNA in multiple sclerosis: search for novel biomarkers. Mult. Scler. 21 (9), 1095–1103. https://doi.org/10.1177/1352458515578771.
Ge, S.X., et al., 2020. ShinyGO: a graphical gene-set enrichment tool for animals and plants. Bioinformatics 36 (8), 2628–2629. https://doi.org/10.1093/bioinformatics/btz931.
González, M.J., et al., 2018. White matter microstructural damage in early treated phenylketonuric patients. Orphanet J. Rare Dis. 13 (1), 188. https://doi.org/10.1186/s13023-018-0912-5.
Gregg, J.R., et al., 2009. Downregulation of oligodendrocyte transcripts is associated with impaired prefrontal cortex function in rats. Schizophr. Res. 113 (2–3), 277–287. https://doi.org/10.1016/j.schres.2009.05.023.
Grisch-Chan, H.M., et al., 2019. State-of-the-art 2019 on gene therapy for phenylketonuria. Hum. Gene Ther. 30 (10), 1274–1283. https://doi.org/10.1089/hum.2019.111.
de Groot, M.J., et al., 2013. Phenylketonuria: reduced tyrosine brain influx relates to reduced cerebral protein synthesis. Orphanet J. Rare Dis. 8 (1), 133. https://doi.org/10.1186/1750-1172-8-133.
de Groot, M.J., et al., 2015. Phenylketonuria: brain phenylalanine concentrations relate inversely to cerebral protein synthesis. J. Cereb. Blood Flow Metab. 35 (2), 200–205. https://doi.org/10.1038/jcbfm.2014.183.
Guerra, I.M.S., et al., 2020. Lipids and phenylketonuria: current evidences pointed the need for lipidomics studies. Arch. Biochem. Biophys. 688, 108431 https://doi.org/10.1016/j.abb.2020.108431.
Hamman, K., et al., 2005. Low therapeutic threshold for hepatocyte replacement in murine phenylketonuria. Mol. Ther. 12 (2), 337–344. https://doi.org/10.1016/j.ymthe.2005.03.025.
Herbert, A.L., et al., 2017. Dynein/dynactin is necessary for anterograde transport of Mbp mRNA in oligodendrocytes and for myelination in vivo. Proc. Natl. Acad. Sci. U. S. A. 114 (43), E9153–E9162. https://doi.org/10.1073/pnas.1711088114.
Hoeksma, M., et al., 2009. Phenylketonuria: high plasma phenylalanine decreases cerebral protein synthesis. Mol. Genet. Metab. 96 (4), 177–182. https://doi.org/10.1016/j.ymgme.2008.12.019.
Hong, S., et al., 2021. Gene expression profiles in the brain of phenylketonuria mouse model reversed by the low phenylalanine diet therapy. Metab. Brain Dis. 36 (8), 2405–2414. https://doi.org/10.1007/s11011-021-00818-0.
Huttenlocher, P.R., 2000. The neuropathology of phenylketonuria: human and animal studies. Eur. J. Pediatr. 159 (Suppl), S102–S106. https://doi.org/10.1007/pl00014371.
Idichi, T., et al., 2017. Regulation of actin-binding protein ANLN by antitumor miR-217 inhibits cancer cell aggressiveness in pancreatic ductal adenocarcinoma. Oncotarget 8 (32), 53180–53193. https://doi.org/10.18632/oncotarget.18261.
Jahn, O., et al., 2020. The CNS myelin proteome: deep profile and persistence after post-mortem delay. Front. Cell. Neurosci. 14, 239. https://doi.org/10.3389/fncel.2020.00239.
Joseph, B., Dyer, C.A., 2003. Relationship between myelin production and dopamine synthesis in the PKU mouse brain. J. Neurochem. 86 (3), 615–626. https://doi.org/10.1046/j.1471-4159.2003.01887.x.
Klippel, B., et al., 2021. White Matter Disturbances in Phenylketonuria: Possible Underlying Mechanisms. (February 2020), pp. 349–360. https://doi.org/10.1002/jnr.24598.
Laursen, L.S., et al., 2011. Translation of myelin basic protein mRNA in oligodendrocytes is regulated by integrin activation and hnRNP-K. J. Cell Biol. 192 (5), 797–811. https://doi.org/10.1083/jcb.201007014.
Li, D., et al., 2010. Effects of phenylalanine on the survival and neurite outgrowth of rat cortical neurons in primary cultures: possible involvement of brain-derived neurotrophic factor. Mol. Cell. Biochem. 339 (1–2), 1–7. https://doi.org/10.1007/s11010-009-0364-2.
Lu, P., et al., 2021. A novel CNTNAP2 mutation results in abnormal neuronal E/I balance. Front. Neurol. 12, 712773 https://doi.org/10.3389/fneur.2021.712773.
Lu, Z., et al., 2005. Developmental abnormalities of myelin basic protein expression in fyn knock-out brain reveal a role of fyn in posttranscriptional regulation. J. Biol. Chem. 280 (1), 389–395. https://doi.org/10.1074/jbc.M405973200.
Lyons, D.A., et al., 2009. Kif1b is essential for mRNA localization in oligodendrocytes and development of myelinated axons. Nat. Genet. 41 (7), 854–858. https://doi.org/10.1038/ng.376.
Mann, S.A., et al., 2008. Corticosteroids reverse cytokine-induced block of survival and differentiation of oligodendrocyte progenitor cells from rats. J. Neuroinflammation 5, 39. https://doi.org/10.1186/1742-2094-5-39.
McDonald, J.D., Charlton, C.K., 1997. Characterization of mutations at the mouse phenylalanine hydroxylase locus. Genomics 39 (3), 402–405. https://doi.org/10.1006/geno.1996.4508.
McKerracher, L., Rosen, K.M., 2015. MAG, myelin and overcoming growth inhibition in the CNS. Front. Mol. Neurosci. 8, 51. https://doi.org/10.3389/fnmol.2015.00051.
Michel, K., et al., 2015. Translational control of myelin basic protein expression by ERK2 MAP kinase regulates timely remyelination in the adult brain. J. Neurosci. 35 (20), 7850–7865. https://doi.org/10.1523/JNEUROSCI.4380-14.2015.
Müller, C., et al., 2013. Making myelin basic protein -from mRNA transport to localized translation. Front. Cell. Neurosci. 7 https://doi.org/10.3389/fncel.2013.00169.
Müller, C., et al., 2015. SncRNA715 inhibits schwann cell myelin basic protein synthesis. PLoS One 10 (8), 1–11. https://doi.org/10.1371/journal.pone.0136900.
Nave, K.-A., Werner, H.B., 2014. Myelination of the nervous system: mechanisms and functions. Annu. Rev. Cell Dev. Biol. 30, 503–533. https://doi.org/10.1146/annurev-cellbio-100913-013101.
Noren Hooten, N., et al., 2013. Age-related changes in microRNA levels in serum. Aging (Albany. NY). 5 (10), 725–740. https://doi.org/10.18632/aging.100603.
Norton, W.T., Poduslo, S.E., 1973. Myelination in rat brain: changes in myelin composition during brain maturation. J. Neurochem. 21 (4), 759–773. https://doi.org/10.1111/j.1471-4159.1973.tb07520.x.
Paraskevopoulou, M.D., et al., 2013. DIANA-microT web server v5.0: service integration into miRNA functional analysis workflows. Nucleic Acids Res. 41 (Web Server issue), W169–W173. https://doi.org/10.1093/nar/gkt393.
Park, J.-W., et al., 2009. Altered brain gene expression profiles associated with the pathogenesis of phenylketonuria in a mouse model. Clin. Chim. Acta 401 (1), 90–99. https://doi.org/10.1016/j.cca.2008.11.019.
Pascucci, T., et al., 2018. A new therapy prevents intellectual disability in mouse with phenylketonuria. Mol. Genet. Metab. 124 (1), 39–49. https://doi.org/10.1016/j.ymgme.2018.03.009.
Patzig, J., et al., 2016. Septin/anillin filaments scaffold central nervous system myelin to accelerate nerve conduction. Elife 5, e17119. https://doi.org/10.7554/eLife.17119 (Edited by B. Stevens).
Preissler, T., et al., 2016. Phenylalanine induces oxidative stress and decreases the viability of rat astrocytes: possible relevance for the pathophysiology of neurodegeneration in phenylketonuria. Metab. Brain Dis. 31 (3), 529–537. https://doi.org/10.1007/s11011-015-9763-0.
Quarles, R.H., 2007. Myelin-associated glycoprotein (MAG): past, present and beyond. J. Neurochem. 100 (6), 1431–1448. https://doi.org/10.1111/j.1471-4159.2006.04319.x.
Rahmanzadeh, R., et al., 2018. Demyelination with preferential MAG loss: a complex message from MS paraffin blocks. J. Neurol. Sci. 385, 126–130. https://doi.org/10.1016/j.jns.2017.12.029.
Rossi, L., et al., 2014. Erythrocyte-mediated delivery of phenylalanine ammonia lyase for the treatment of phenylketonuria in BTBR-Pah(enu2) mice. J. Control. Release 194, 37–44. https://doi.org/10.1016/j.jconrel.2014.08.012.

Schäfer, I., et al., 2016. MOBP levels are regulated by Fyn kinase and affect the morphological differentiation of oligodendrocytes. J. Cell Sci. 129 (5), 930–942. https://doi.org/10.1242/jcs.172148.
Schoemans, R., et al., 2010. Oligodendrocyte development and myelinogenesis are not impaired by high concentrations of phenylalanine or its metabolites. J. Inherit. Metab. Dis. 33 (2), 113–120. https://doi.org/10.1007/s10545-010-9052-3.
Schuck, P.F., et al., 2015. Phenylketonuria pathophysiology: on the role of metabolic alterations. Aging Dis. 6 (5), 390–399. https://doi.org/10.14336/AD.2015.0827.
Scott, R., et al., 2019. Loss of Cntnap2 causes axonal excitability deficits, developmental delay in cortical myelination, and abnormal stereotyped motor behavior. Cereb. Cortex 29 (2), 586–597. https://doi.org/10.1093/cercor/bhx341.
Shannon, P., et al., 2003. Cytoscape: a software environment for integrated models of biomolecular interaction networks. Genome Res. 13 (11), 2498–2504. https://doi.org/10.1101/gr.1239303.
Shefer, S., et al., 2000. Is there a relationship between 3-hydroxy-3-methylglutaryl coenzyme a reductase activity and forebrain pathology in the PKU mouse? J. Neurosci. Res. 61 (5), 549–563. https://doi.org/10.1002/1097-4547(20000901)61:5<549::AID-JNR10>3.0.CO;2-0.
Smirnova, E.V., et al., 2021. Comprehensive atlas of the myelin basic protein interaction landscape. Biomolecules 11 (11). https://doi.org/10.3390/biom11111628.
Smith-Vikos, T., Slack, F.J., 2012. MicroRNAs and their roles in aging. J. Cell Sci. 125, 7–17. https://doi.org/10.1242/jcs.099200.
Solly, S.K., et al., 1996. Myelin/oligodendrocyte glycoprotein (MOG) expression is associated with myelin deposition. Glia 18 (1), 39–48. https://doi.org/10.1002/(SICI)1098-1136(199609)18:1<39::AID-GLIA4>3.0.CO;2-Z.
van Spronsen, et al., 2009. Brain dysfunction in phenylketonuria: is phenylalanine toxicity the only possible cause? J. Inherit. Metab. Dis. 32 (1), 46–51. https://doi.org/10.1007/s10545-008-0946-2.
van Spronsen, F.J., et al., 2021. Phenylketonuria. Nat. Rev. Dis. Prim. 7 (1), 36. https://doi.org/10.1038/s41572-021-00267-0.
Stadelmann, C., et al., 2019. Myelin in the central nervous system: structure, function, and pathology. Physiol. Rev. 99 (3), 1381–1431. https://doi.org/10.1152/physrev.00031.2018.
Szklarczyk, D., et al., 2019. STRING v11: protein–protein association networks with increased coverage, supporting functional discovery in genome-wide experimental datasets. Nucleic Acids Res. 47 (D1), D607–D613. https://doi.org/10.1093/nar/gky1131.
Tao, R., et al., 2020. Long-term metabolic correction of phenylketonuria by AAV-delivered phenylalanine amino Lyase. Mol. Ther. - Methods Clin. Dev. 19, 507–517. https://doi.org/10.1016/j.omtm.2019.12.014.
Thau-Zuchman, O., et al., 2022. High phenylalanine concentrations induce demyelination and microglial activation in mouse cerebellar organotypic slices. Front. Neurosci. 16, 926023 https://doi.org/10.3389/fnins.2022.926023.
Torvund-Jensen, J., et al., 2014. Transport and translation of MBP mRNA is regulated differently by distinct hnRNP proteins. J. Cell Sci. 127 (Pt 7), 1550–1564. https://doi.org/10.1242/jcs.140855.
Umemori, H., et al., 1994. Initial events of myelination involve Fyn tyrosine kinase signalling. Nature 367 (6463), 572–576. https://doi.org/10.1038/367572a0.
Umemori, H., et al., 1999. Stimulation of myelin basic protein gene transcription by Fyn tyrosine kinase for myelination. J. Neurosci. 19 (4), 1393–1397. https://doi.org/10.1523/JNEUROSCI.19-04-01393.1999.
Wang, S., et al., 2020. Ermin is a p116(RIP) -interacting protein promoting oligodendroglial differentiation and myelin maintenance. Glia 68 (11), 2264–2276. https://doi.org/10.1002/glia.23838.
White, R., et al., 2008. Activation of oligodendroglial Fyn kinase enhances translation of mRNAs transported in hnRNP A2-dependent RNA granules. J. Cell Biol. 181 (4), 579–586. https://doi.org/10.1083/jcb.200706164.
Winn, S.R. et al., 2022. Modeling the cognitive effects of diet discontinuation in adults with phenylketonuria (PKU) using pegvaliase therapy in PAH-deficient mice. Mol. Genet. Metab. [Preprint]. doi: https://doi.org/10.1016/j.ymgme.2022.03.008.
Winn, S.R., et al., 2016. High dose sapropterin dihydrochloride therapy improves monoamine neurotransmitter turnover in murine phenylketonuria (PKU). Mol. Genet. Metab. 117 (1), 5–11. https://doi.org/10.1016/j.ymgme.2015.11.012.
Winn, S.R., et al., 2018. Blood phenylalanine reduction corrects CNS dopamine and serotonin deficiencies and partially improves behavioral performance in adult phenylketonuric mice. Mol. Genet. Metab. 123 (1), 6–20. https://doi.org/10.1016/j.ymgme.2017.10.009.
Yu, Y.G., et al., 2007. Effects of phenylalanine and its metabolites on cytoplasmic free calcium in cortical neurons. Neurochem. Res. 32 (8), 1292–1301. https://doi.org/10.1007/s11064-007-9303-3.
Ziaei, A., et al., 2022. Ermin deficiency leads to compromised myelin, inflammatory milieu, and susceptibility to demyelinating insult. Brain Pathol. 32 (5), 1–19. https://doi.org/10.1111/bpa.13064.